AN ABSTRACT OF THE THESIS OF

Hai Yang for the degree of Master of Science in Wood Science and Engineering presented on June 21, 2012

Title: Modeling the Fixed Bed Drying Characteristics of Biomass Particles

Abstract approved: _____
Michael R. Milota

The fixed bed drying of western hemlock and Douglas-fir biomass particles at temperatures ranging from 50°C to 200°C and air velocities from 0.3 to 0.9 m/s was investigated. The objectives were to describe the drying characteristics of the particles, fit a model for thin-layer drying, and develop and test a deep bed drying model based on the thin-layer model.

The effects of temperature and air velocity were determined in a bed approximately 1.3 cm in depth and a model for the drying curve was developed. The thin-layer model was then used to predict what would happen in a deeper bed. Model results were compared to drying curves measured in a 23-cm-deep bed. The deep bed model predicted both the experimental drying times and the moisture and temperature profiles in the bed.

©Copyright by Hai Yang
June 21, 2012
All Rights Reserved

Modeling the Fixed Bed Drying Characteristics of Biomass Particles

by
Hai Yang

A THESIS

Submitted to

Oregon State University

in partial fulfillment of
the requirements for the
degree of

Master of Science

Presented June 21, 2012
Commencement June 2013

Master of Science thesis of Hai Yang presented on June 21, 2012.

APPROVED:

_____

Major Professor, representing Wood Science and Engineering

_____

Head of the Department of Wood Science and Engineering

_____

Dean of the Graduate School

I understand that my thesis will become part of the permanent collection of Oregon State University libraries. My signature below authorizes release of my thesis to any reader upon request.

_____

Hai Yang, Author

ACKNOWLEDGEMENTS

I would like to express my gratitude to many individuals. I could not be more thankful to my major professor, Dr. Michael R. Milota, for his meaningful guidance, invaluable insight, and always positive encouragement. I am grateful to him for bringing me into this project, as I learned so much from him and enjoyed studying and working with him. I would also like to acknowledge David Smith for his suggestions and help with the experiments.

My special thanks also go to my minor professor, Dr. Lan Xue, for her support, as well as my committee members, Dr. Scott Leavengood and Dr. David Woodruff, for their encouragement and help.

Gratitude must be expressed to my friends Jie Ding, Dr. Xiaofeng Ren and Jesse Paris for help whenever I needed it, and all the students, faculty, and staff in the Wood Science and Engineering department.

Many thanks go to my friends Yu Li and Cheng Li for helping me with the statistic data analysis, and all my friends, faculty, and staff in Statistic department. I extend many thanks to the people in my basketball and hiking groups in Corvallis; my life will not be so colorful without you guys. Also thanks to my great friends back in China for their sincere and supportive help. Finally, I would love to express my exceptional thanks to my family, for their unconditional love and support.

TABLE OF CONTENTS

Contents Page

CHAPTER 1. Introduction 1

1.1 Background and problem statement 1

1.2 Statement of objectives 2

1.3 Methodology 3

CHAPTER 2. Literature Review 5

2.1 Woody biomass as a renewable fuel 5

2.1.1 Benefit of woody biomass fuel 6

2.1.2 Negatives of using woody biomass fuel 7

2.2 Woody biomass drying 7

2.2.1 Important of woody biomass drying 8

2.2.2 Woody biomass product and utilization 8

2.3 Woody biomass drying process 8

2.3.1 Materials 9

2.3.2 Equipment 11

2.3.3 Factors affecting the drying rate 16

2.3.4 Thin-layer dryer model description 21

2.3.5 Deep bed drying analysis 23

CHAPTER 3. Material and Methods 27

3.1 Material 27

3.1.1 Particle size 27

TABLE OF CONTENTS (Continued)

3.1.2 Initial moisture content....28

3.2 The drying equipment 29

3.2.1 Dryer gas supply....29

3.2.2 Dryer configuration 30

3.2.3 Instrumentation....32

3.2.4 Control....33

3.3 Thin-layer experiments 35

3.3.1 Drying procedure....35

3.3.2 Experimental design 36

3.3.3 Calculations to determine drying curve....38

3.3.4 Model development....38

3.4 Deep-layer experiment 40

3.4.1 Drying procedure....40

3.4.2 Experimental design 41

3.4.3 Calculations 42

CHAPTER 4. Results and Analysis 44

4.1 Wood description 44

4.1.1 Size distribution....44

4.1.2 Initial moisture content....45

4.2 Thin-layer drying.... 45

4.2.1 Effect of Temperature....46

TABLE OF CONTENTS (Continued)

4.2.2 Effect of Velocity 48

4.2.3 Other effects 51

4.2.4 Modeling thin layer drying 56

4.3 Deep-bed drying 65

4.3.1 Experimental bed behavior 65

4.3.2 Effect of drying parameters 67

4.3.3 Drying rate and drying zone 74

4.3.4 Modeling bed drying 82

CHAPTER 5. Conclusions 95

Bibliography 96

Appendices 99

Appendix 1: Statistical analysis for the models 99

Appendix 2: SAS code used for models one to eight. 104

Appendix 3: R code used for two models and pseudo R^2 106

Appendix 4: Example form for manually-recorded data..... 108

Appendix 5: Data automatically recorded by LabView. 110

LIST OF FIGURES

Figure Page

Figure 2.1 Summary of potentially available forest resources (Perlack et al. 2005). 6

Figure 2.2 Effect of water content on lower heating value (LHV) of wood (EUBIA 2007). 12

Figure 2.3 Sketch of a bed dryer. 14

Figure 2.4 Thin-layer and deep bed. 15

Figure 2.5 Schematic of drying and measuring equipment (Bengtsson 2008). 15

Figure 2.6 The drying zone progression through the bed material (Bengtsson 2008). 20

Figure 2.7 Drying characteristic functions of MC, drying rate and temperature with time (Mujumdar 1987). 24

Figure 2.8 Drying rate curve with drying moisture content (Mujumdar 1987). 25

Figure 2.9 Comparison of measured and calculated values of moisture content for aspen chips (Yrjola 2002). 26

Figure 3.1 Oscillating shaker and wood chips on basket. 28

Figure 3.2 Experimental drying equipment. 30

Figure 3.3 A. outside view of drying chamber drying chamber (left); B. inside view of drying chamber (right). 32

Figure 3.4 Labview operating panel.....34

Figure 4.1 Three replicates of experiment data for hemlock at 50°C and 0.6 m/s. .46

Figure 4.2 Effect of temperature on drying time in thin-layer drying. 47

Figure 4.2 Effect of temperature on drying time in thin-layer drying (continued). .48

Figure 4.3 Effect of drying air velocity on drying time in thin-layer drying. 49

LIST OF FIGURES (Continued)

Figure 4.3 Effect of drying air velocity on drying time in thin-layer drying (continuted). 50

Figure 4.3 Effect of drying air velocity on drying time in thin-layer drying (continued). 51

Figure 4.4 Effect of particle size at the same drying condition on drying time. 52

Figure 4.4 Effect of particle size at the same drying condition on drying time (continued). 53

Figure 4.5 Moisture ratios versus drying time for different species at the same drying conditions. D.F. means Douglas-fir 54

Figure 4.5 Moisture ratios versus drying time for different species at the same drying conditions. D.F. means Douglas-fir (continued) 55

Figure 4.6 Comparison of the fitted parameter k (ordinate) to the experimental values (abscissa) for each experiment. 63

Figure 4.7 Predicted moisture content plotted with the experimental data for thin layer drying. 63

Figure 4.7 Predicted moisture content plotted with the experimental data for thin layer drying (continued). 64

Figure 4.8 Load cell output and total weights versus drying time. 66

Figure 4.9 Average bed moisture content versus time for deep bed drying. 67

Figure 4.10 Temperatures at six bed and dryer locations versus drying time.....68

Figure 4.11 Effect of drying air temperature on drying time in deep bed drying. ...69

Figure 4.11 Effect of air temperature on drying time in deep bed drying (continued). 70

Figure 4.12 Effect of air velocity on drying time in deep bed drying.....71

Figure 4.12 Effect of drying air velocity on drying time in deep bed drying (continued). 72

Figure 4.13 Drying comparisons of Douglas-fir and hemlock by moisture ratio. ...73

LIST OF FIGURES (Continued)

Figure 4.14 Drying comparisons of Douglas-fir and hemlock by drying rate. 74

Figure 4.15 Drying rate as a function of time (A) and moisture content (B) for a bed inlet temperature of 100°C and an air velocity of 0.61 m/s. 76

Figure 4.16 Ideal drying curve and measured point. 77

Figure 4.17 Plot of drying zone velocity versus temperature at different air velocities 80

Figure 4.18 Plot of drying zone width versus temperature with groups of velocity. 82

Figure 4.19 Dry bulb temperatures, wet bulb temperature and air velocity. 84

Figure 4.20 Predicted moisture content versus time for deep bed drying. 84

Figure 4.21 Moisture content at each layer at the end of drying. 85

Figure 4.22 Gas temperature at each depth at the end of drying. 85

Figure 4.23 Comparison of experiment curve with predicted curve showing the effect of air velocity on drying time. 90

Figure 4.23 Comparison of experiment curve with predicted curve showing the effect of air velocity on drying time (continued). 91

Figure 4.24 Comparison of experiment curves with predicted curves showing the effect of temperature on drying time. 92

Figure 4.24 Comparison of experiment curves with predicted curves showing the effect of temperature on drying time (continued). 93

Figure 4.25 Comparison of experiment curve with predict curve on effect of species on drying time. 93

LIST OF TABLES

Table Page

Table 2.1 Wood chips and sources (Wikipedia 2012). 9

Table 2.2 Initial moisture content ranges of each type of raw material (EUBIA 2007). 10

Table 2.3 Dryer classifications (Roos 2008). 12

Table 2.4 Dryer type comparison (Roos 2008). O&M is operating and maintenance. 13

Table 2.5 Arithmetic average of particle characteristics for screened and unscreened material dried in the batch fluidized-bed dryer (Milota and Wilson 1989). 19

Table 2.6 Available models for thin-layer drying (Ertekin and Yaldiz 2004). 22

Table 3.1 Experimental design to determine the drying curves for the thin-layer drying. 37

Table 3.2 Deep bed drying experimental design for factors effect on drying time. 42

Table 4.1 Size distribution of hemlock chips. 44

Table 4.2 Initial moisture content of wood. 45

Table 4.3 Statistical analysis results of the models by average RMSE and adjust R^2. 57

Table 4.4 Values of k for each experiment. 58

Table 4.5 Parameter for k based on several models for temperature and air velocity 59

Table 4.6 Fitted and experimentally-determined values for k in the order of increasing temperature. 61

Table 4.7 Average difference percent between fitted and experimental-determined values for k. 62

Table 4.8 Data of drying zone speed and drying zone width. 79

LIST OF TABLES (Continued)

Table 4.9 Drying zone width predict by deep layer model. 81

Table 4.10 Predicted and experimental data for a final moisture content of 12%. ..87

Table 4.11 Predicted and experimental data for a final moisture content of 7%. 88

Modeling the Fixed Bed Drying Characteristics of Biomass Particles

CHAPTER 1. Introduction

1.1 Background and problem statement

Global production of biomass and biofuel are growing rapidly due to increases in the price of fossil fuels and growing environmental concerns. As a renewable material, biomass is also regarded as a pathway to national security and a way to diversify the sustainability of the energy supply. Energy from biomass in the US has the potential to replace 30% of the 2005 petroleum consumption (Perlack et al. 2005).

The 2006 EU Forest Action Plan calls for increasing use of forest biomass for energy (Stupak et al. 2007). The U.S. has enacted regulations or even adopted aggressive goals to encourage increased usage of biofuels. Similarly, the Energy Independence and Security Act of 2007 in the U.S. calls for increased use of renewable energy, including from woody sources (Sissine 2007).

Converting biomass to energy can have several advantages. For example, biomass is also considered a carbon neutral fuel source. Removing forest biomass can reduce fire risk and improve the health of the forest. Moreover, wood may be less expensive than many fossil fuels for short to mid-distance transportation (Bartuska 2006). On the other hand, there are also disadvantages related to the use

of wood as an energy source. For instance, the price of wood is particularly variable. In addition, transportation and storage of woody biomass are expensive.

Improving the utilization of forest resources, particularly as it relates to the production of energy and bio-based products, is critical at the current time. Drying is often the first step to convert biomass to biofuel or bio-products which have to meet requirements for moisture content (MC). For wood-fired incineration, the optimum MC is 10~15%, the final MC should less than 20% for most gasifiers, and the optimum MC is less than 15% to produce stable and durable pellets (Roos 2008). Densification requires low moisture content, often in the 8-10% range. Drying can also reduce the cost of transportation as more material can be placed on a truck.

There is still a lack of information regarding the drying characteristics of residues, and the drying curves for several particle types are not available now. Therefore, a research project intended to study, in detail, the drying characteristics and drying curves of particle needs to be developed. Additionally, this research should analyze the main effect of several variables in the drying process, such as temperature, air velocity, species, and finally develop a thin-layer and deep bed drying model.

1.2 Statement of objectives

The objectives of this research are to evaluate the drying characteristics of wood particles, develop thin-layer drying model that describes the particle behavior,

and develop a deep bed drying model for wood residues. Thus, this study is intended to

- Determine the effect of drying air temperature on drying time
- Determine the effect of drying air velocity on drying time
- Determine the effect of particle size on drying time
- Determine the effect of species on drying time
- Find a model that can most fit the drying curves observed in this study
- Develop a thin-layer drying model
- Develop a deep bed drying model based on the thin-layer model
- Describe the vertical temperature profile during the deep bed drying process.
- Describe the vertical moisture content profile during the deep bed drying process.

1.3 Methodology

In order to achieve the research goal, the thesis will be divided into 5 chapters.

Chapter 1 Introduction. This defines the problem to study in this research. The objective and importance of this study are also stated in this chapter. A basic background for this research is covered as well.

Chapter 2 Literature Review. This contains the background needed to carry out this study, which is divided into three sections. Each of these sections is focused on the fundamental manufacturing operations that are necessary to drying wood residues, that

is: renewable fuel source, fundamentals of drying, and drying process. The chapter is based on papers, technical literature, and publications linked to the topics just mentioned.

Chapter 3 Material and Methods. This identifies and defines the most important variables for this study. The equipment used in the study is described. This chapter also describes how the variables are monitored, measured, or controlled.

Chapter 4 Results and Analysis. This shows data that is collected from the experiments. In this section, the results obtained from experimentation are discussed. Explanations of these results are also provided based on the background developed in Chapter 2.

Chapter 5 Conclusions. Achievements and facts of this research are shown in this chapter.

Bibliography. This chapter lists the literature cited in this project, such as books, papers, publications, technical literature, etc.

Appendices. Supplementary material regarding this project is presented in the appendices.

CHAPTER 2. Literature Review

This chapter presents the necessary background to explain the research. It is focused on the woody biomass fuel source and describes the fundamental concepts of the biomass drying process. Additionally, since the main objective of this project is to develop thin-layer drying model and deep bed drying model to find the best fit parameters for most biomass drying situations, previous work on woody biomass associated with thin-layer drying and deep bed drying are also discussed.

2.1 Woody biomass as a renewable fuel

Forestland-derived biomass has the potential to produce approximately 368 million dry tons annually (Perlack et al. 2005) in the U.S. Two major sources are 145 million dry tons of residues from wood processing and pulp and paper mills and 64 million dry tons of residues from logging and site clearing operations. Figure 2.1(Perlack et al. 2005)continues a further breakdown of these sources.

About 60% of the total harvested tree is left in forest (FAO 1982) (cited by Parikka (2004)) and 50% of softwood log brought to a sawmill is produced into lumber (Milota et al. 2005).

Woody biomass energy can be converted into electricity, heat or processed fuels (Hewett 1981) by direct burning, pyrolysis, or gasification. The most effective process to convert woody biomass to energy is by direct burning (Zerbe 2006).

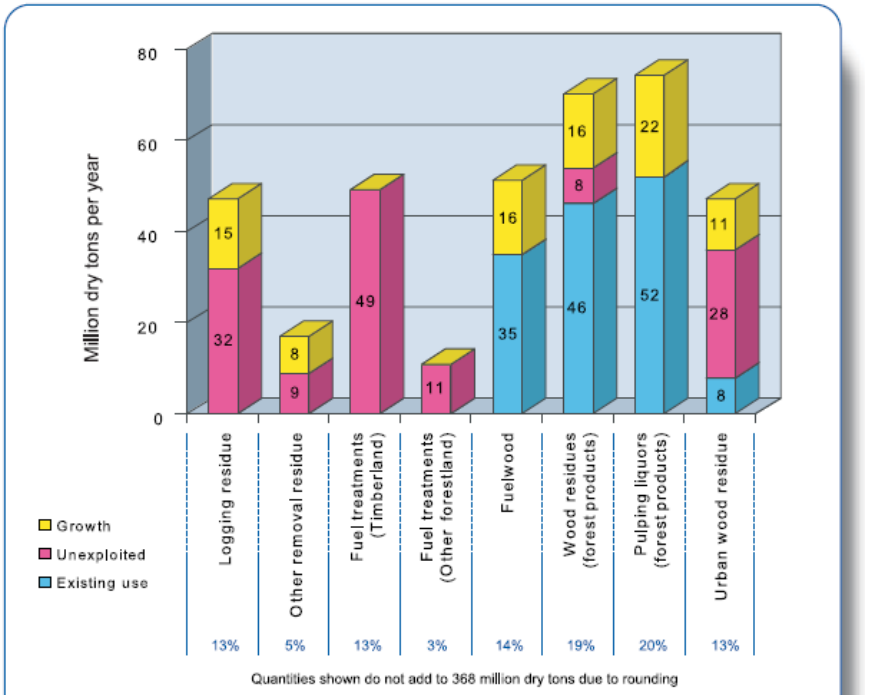

Figure 2.1 Summary of potentially available forest resources (Perlack et al. 2005).

2.1.1 Benefit of woody biomass fuel

The benefit of using woody biomass can be divided into energy, environmental, and economic benefits.

Energy from the biomass in the U.S. has the potential to replace 30% of the 2005 petroleum consumption(Perlack et al. 2005). Woody biomass fuel combined with short to mid-term transportation is technically possible (Bartuska 2006). Woody biomass energy also improves national energy security by reducing dependence on foreign oil.

Environmental benefits can be achieved by removing forest biomass to reduce fire risk and improve the health of the forest. Woody biomass is sustainable and renewable, which is friendly to the environment. There is no net increase in atmospheric CO_2 though the use of woody fuel compared to fossil fuel, which makes the biomass fuel a green fuel. Biomass fuel can play an important role in a future green environment.

Economic benefits of using woody biomass fuel include creating jobs in rural areas and providing opportunities for rural economies to grow and expand. Biomass utilization can also reduce forest management cost and make the forest more healthy (Bartuska 2006).

2.1.2 Negatives of using woody biomass fuel

There are some negative consequences of using wood as fuel. The price of wood fuel can be extremely variable. Transportation costs are usually in range of $0.2 to 0.6 per dry ton-mile and could severely limit haul distances. A large space is needed to store wood because it has a lower energy density compared to fossil fuel. Lower combustion efficiency and increased particulate emissions are also negatives (Hakkila 1989).

2.2 Woody biomass drying

Drying refers to the reduction of the amount of water in wood. The main objective is to achieve desired moisture content in the material at the end of the drying process and to have this be uniform.

2.2.1 Important of woody biomass drying

There are several reasons why drying biomass is desirable. Transportation costs may be reduced if drying is done close to the harvest site. Wood is less likely to degrade due to biological action in storage when the wood is dry. Combustion efficiencies are greater when dry fuel is burned compared to wet. For example, the maximum boiler efficiency with standard equipment is about 74%, using wood chips with a moisture content of 45%; while the efficiency can increase to 80% when using the wood with a moisture of 10-15% (Roos 2008). The reason for the combustion efficiency increase is that dry wood burns at a flame temperature of 2300-2500° F, while green wood burns at about 1800° F.

2.2.2 Woody biomass product and utilization

Pellets, briquettes, fire logs are made to burn to reduce transportation and handing costs. In addition to direct combustion, there are a number of products that could be produced from woody biomass. Some examples include composites, landscaping products, and paper.

2.3 Woody biomass drying process

The principle of drying wood particles is to remove the water rapidly by putting them through a high temperature drying medium (Maloney 1993). One controlled temperature or series of temperatures are used for a specified time. The exact parameters depend on the physical properties and characteristics of the product (Corder 1958).

2.3.1 Materials

Types of raw material, initial and final moisture contents of the raw material, and the particle size and geometry are important factors that should be considered on drying biomass.

2.3.1.1 Wood chips and its resource

Shown in Table 2.1 are wood chips and a list of possible sources.

Table 2.1 Wood chips and sources (Wikipedia 2012).

picture	Woodchips Source
	Waste wood and residuals from construction, agriculture, landscaping, logging, and sawmills. Locally grown and harvested fuel crops.

2.3.1.2 Particle geometry

The size and shape of the particles to be dried are also important factors that affect drying process. Since the main object of any drying operation is to reduce the moisture content of the material being dried, increasing the size of the particles of a given shape will tend to increase the cost of drying (Maloney 1993). The size of

wood particles is determined by the diameters of screen holes, and the hog fuel pieces run between coarse grades of less than 5" to a fine grade of less than 2".

2.3.1.3 Initial moisture content

Some parameters have to be taken into consideration when evaluating the initial moisture content (MC) of the raw material: First, the source of the raw material as shown in Table 2.2 should be considered. Wood particles coming from a secondary manufacturing process will have lower moisture content (MC) than those from green wood. Second, wood species has a significant effect on the green moisture content of raw material (Maloney 1993). For example, the green MC of pines is between 80 and 200% (oven-dried basis) while green Douglas-fir is about 40% (Maloney 1993). Third, variation in the initial moisture content is also important.

Table 2.2 Initial moisture content ranges of each type of raw material (EUBIA 2007).

Biomass resource	Moisture content
Industrial fresh wood chips and sawdust	40-60 wt. % (wb)
Industrial dry wood chips and sawdust	10-20 wt. % (wb)
Fresh forest wood chips	40-60 wt. % (wb)
Chips from wood stored and air-dried several months	30-40 wt. % (wb)
Waste wood	10-30 wt. % (wb)

2.3.1.4 Final moisture content

Final moisture content requirements are different among different products. The average ending MC should meet the product requirements. If over-drying occurs, it means wasting energy. If final MC is higher than the requirement it will lead to lower energy density and decrease the combustion efficiency.

2.3.1.5 The relationship between energy density and the moisture content

With an increase in MC, the woody biomass will have a lower energy density. Figure 2.2 shows the relationship between MC and energy density. The water content means moisture content.

2.3.2 Equipment

2.3.2.1 Traditional equipment

Biomass dryers can be classified as several types: direct- and indirect-fired rotary dryers, conveyor dryers, cascade dryers, flash or pneumatic dryers, superheated steam dryers, and microwave dryers. There are many factors to be considered when selecting the appropriate dryer, including the size and characteristics of the feedstock, capital cost, operation and maintenance requirements, environmental emissions, energy efficiency, waste heat sources available, available space, and potential fire hazard (Roos 2008).

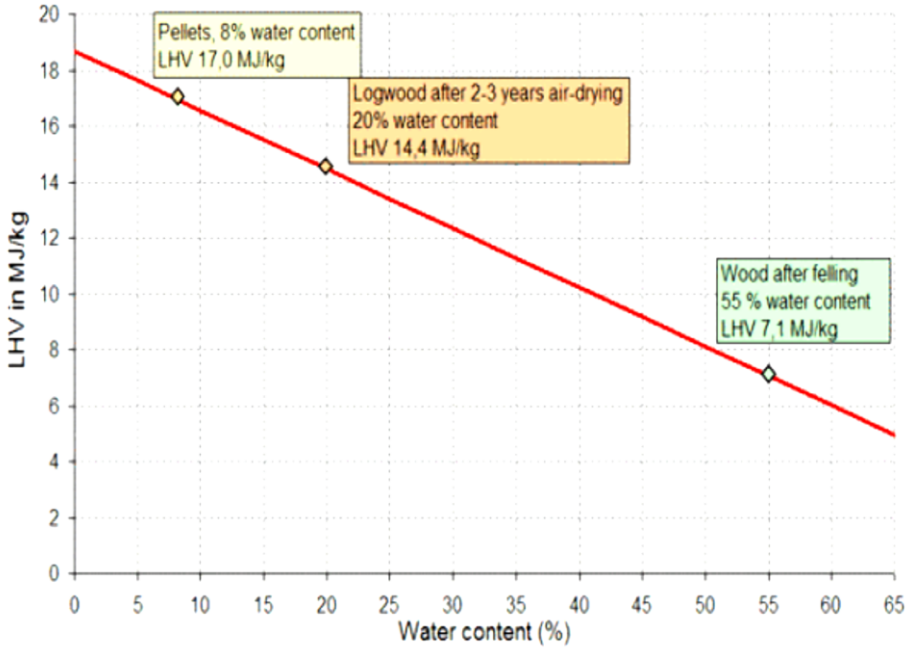

Figure 2.2 Effect of water content on lower heating value (LHV) of wood (EUBIA 2007).

Table 2.3 Dryer classifications (Roos 2008).

Classification	Alternatives
Drying media (i.e. the stream passing through the material to be dried)	Flue gas, hot air or superheated steam
Firing	Direct- or indirect-fired
Heat transfer media	Flue gas, hot air, steam, or hot water
Pressure	Atmospheric, vacuum or high pressure
Heat source	Dryer burners, boiler (flue gas or steam), recovered waste heat from facility processes

Table 2.4 Dryer type comparison (Roos 2008). O&M is operating and maintenance.

Dryer Type	Feedstock Requirements	Capital & Operating Cost	O&M Requirements	Environmental Emissions	Energy Efficiency & Heat Recovery	Footprint
Rotary	Less sensitive to particle size. High content paper sludges tend to ball up. Coarse bark can be problematic.		Low	More VOC emissions compared to lower temp dryers	Less opportunity to recover waste heat	
Conveyor	Fines may need to be screened out first and added back.	Comparable to rotary dryer, but may require less ancillary equipment for treatment of emissions reducing overall cost.	Greater than for rotary dryer.	Lower emissions of VOCs and particulates	High opportunity for heat recovery due to lower temperature.	Larger than comparably-sized rotary dryer. Multi-pass conveyors save space and can have comparable footprint to rotary dryer.
Cascade	Requires fairly uniform particle size. Can handle large particle size.	Higher than rotary dryers.	Subject to corrosion and erosion		Heat recovery is difficult. High blower costs.	Smaller footprint than rotary and conveyor dryers.
Flash	Requires small particle size.	Higher than rotary dryers.	Subject to corrosion and erosion		Heat recovery is difficult. High blower costs.	Smaller footprint than rotary and conveyor dryers.
Superheated Steam	Requires small particle size.	High.	High. Subject to corrosion.	No air emissions. Condensate requires treatment.	Very efficient if low-pressure steam is recovered. No heat losses from heating air.	Smaller footprint than rotary and conveyor dryers.

Roos (2008) gives a summary of dryer classifications and compares dryer types, which make it easier to find the best dryer. These are detailed in Table 2.3 and Table 2.4.

2.3.2.2 Thin-layer dryer and deep-layer dryer

The traditional dryers have high cost and low efficiency for small communities who want to install a small-scale dryer to utilize forest biomass. So a dryer which is low-cost and energy efficient is needed for the rural area. The bed

dryer is a simple, low-cost dryer mostly using in drying foods and may fulfill this need. The basic principle of a bed dryer is that hot air comes through the particles, removing the moisture from the wood, as shown in Figure 2.3. The bed dryer has the advantages of simple construction, low electricity demands, and the ability to dry a wide range of sizes and types of residuals (Bengtsson 2008).

Classified by the depth of particles, the bed dryer can be divided into two types: thin-layer dryer and deep-layer dryer. There is not an exact depth of particle between thin-layer and deep bed. A deep bed is a series of thin layers as shown in Figure 2.4.The gas temperature, gas velocity, and gas humidity entering each layer depends on the inlet conditions and the drying that occurred in lower layers. One experimental bed dryer configuration developed by Bengtsson (2008) is shown in Figure 2.5.

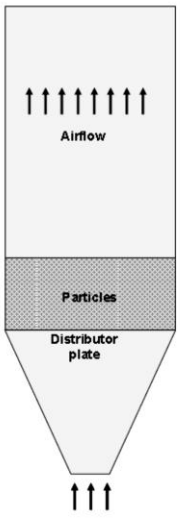

Figure 2.3 Sketch of a bed dryer.

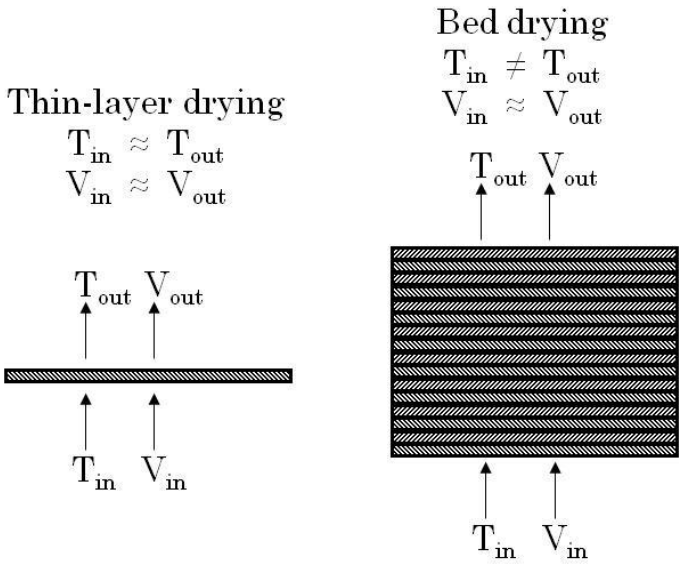

Figure 2.4 Thin-layer and deep bed.

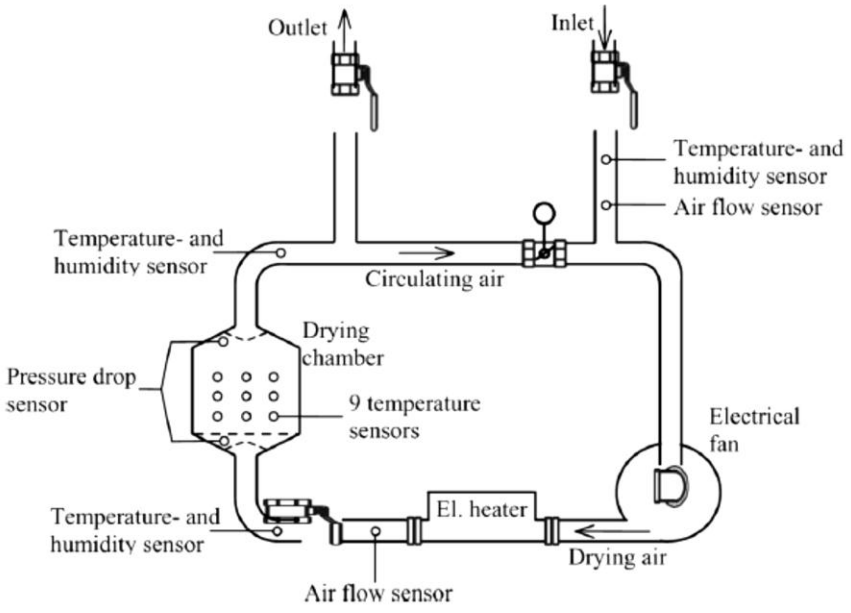

Figure 2.5 Schematic of drying and measuring equipment (Bengtsson 2008).

2.3.3 Factors affecting the drying rate

Drying can be divided into two stages: constant-rate drying at high moisture content and falling-rate drying at low moisture content. Several factors affect the drying rate, such as air velocity, temperature, and geometry of wood.

2.3.3.1 Air flow

For lumber, the drying rate increases with the square root of velocity during the constant period, while air velocity has almost no effect to the falling-rate period (Mujumdar 1987).

$$\frac{Rate_2}{Rate_1} = \sqrt{\frac{V_2}{V_1}} \qquad \text{Equation 2-1}$$

For wood chips, Bengtsson (2008) got a different result in deep bed drying: the length of constant-rate drying period increases between 189 and 246% when the air velocity decreases from 0.28 m/s to 0.22 m/s; the length of falling-rate drying period increases by between 178 and 281% when the air velocity decreases from 0.28 m/s to 0.22 m/s. The effect of air flow in the falling-rate is different between timber drying and Bengtsson's (2008) particle drying tests. Bengtsson (2008) gives the reason of difference is probably an effect of the accuracy of airflow meters. The reason need to test and confirm in this study.

2.3.3.2 Temperature

The drying temperature almost has no effect on constant-rate drying, but has a positive relationship with drying rate during the falling-rate period. The relationship can be expressed using an Arrhenius relationship (Mujumdar 1987).

The Arrhenius expression:

$$\frac{Rate_2}{Rate_1} = \exp\left[\frac{-H}{RT_2} - \frac{-H}{RT_1}\right] \qquad \text{Equation 2-2}$$

where

- H is the activation energy (J kg^{-1} $mole^{-1}$),
- R is the gas constant (J kg^{-1} $mole^{-1}$ K^{-1}),
- T is the absolute temperature (K),
- $Rate_1$ is the drying rate at T_1 (kg/s), and
- $Rate_2$ is the drying rate at T_2 (kg/s).

For wood chips, Bengtsson (2008) determined that, the length of the constant-rate drying period increased by approximately 15% when the air temperature decreased from 92℃ to74℃; the falling-rate drying period increased by between 148 and 241% as the air temperature decreased from 92℃ to74℃. There is not a clear reason in Bengtsson (2008)'s paper to explain why the temperature have an effect on constant-rate period.

2.3.3.3 Particle geometry

Due to the irregularity of biomass particles, Moreno et al. (2004) choose Ergun's equation to find the specific surface of particles. For non-spherical particles, Ergun's equation can be written as follows:

$$\frac{\Delta p}{L} = 150\frac{(1-\varepsilon)^2}{\varepsilon^3}\frac{\mu_g U}{36}S_p^2 + 1.75\frac{1-\varepsilon}{\varepsilon^3}\frac{GU}{6}S_p \qquad \text{Equation 2-3}$$

where: Δ p is the pressure drop in the bed in Pa; L is the height of the static bed in m; ε is the voidage of the bed in m^3m^{-3}; μ_g is the viscosity of the gas in Pa s; U is the superficial velocity of gas in ms^{-1}; G is the mass flux of gas in kg $s^{-1}m^{-2}$; and S_p is the specific surface of the particle in m^2m^{-3}. The specific surface results of two groups of wood chips are: 6530 m^2m^{-3} with a standard deviation of 197 m^2m^{-3} for 1.44 mm particles and 5811 m^2m^{-3} with a standard deviation of 111 m^2m^{-3} for 3.56 mm particles. Moreno et al. (2004) infer that the high particle surface area exposed to fluid may cause high rates of convective heat transfer, but they provide no data to support this.

Milota and Wilson (1989) make a good summary of particle geometry in hammermilled wood particles and sawdust particles. They screened the particles into three groups (small, medium, large). And the "unscreened" furnish is composed of 30% small, 55% medium and 15% large particles by weight.

Table 2.5 Arithmetic average of particle characteristics for screened and unscreened material dried in the batch fluidized-bed dryer (Milota and Wilson 1989).

Particle size class, by type	Screening		Hammermilled wood particles			Sawdust particles		
	Sweco mesh	Larger opening (mm)	Diameter[1] (mm)	Sphericity[2]	Voidage[3]	Diameter (mm)	Sphericity	Voidage
Screened								
Small	+6	—	0.68	0.60	0.49	0.80	0.64	0.45
Medium[4]	−6 + 12	3.35	2.03	0.51	0.54	2.18	0.68	0.53
Large	−12	1.53	3.78	0.46	0.68	4.16	0.47	0.71
Unscreened								
Mixed	—	—	1.33	0.56	0.50	1.51	0.64	0.53

[1] Diameter of a sphere with the same volume as the particle.
[2] Area of a sphere with the same volume as the particle, divided by actual particle area; equals 1 for a sphere and decreases with deviation from roundness.
[3] Fraction of the open area between particles; voidage presented is for beds with no airflow.
[4] Passes through a 3.35-mm screen but is retained by a 1.53-mm screen.

Characteristics of each size class are summarized in Table 2.5. To deal with the irregular shape of particles, they use the diameter of sphere with the same volume as particle.

2.3.3.4 Depth of drying

The drying period is increased as the depth of the particles increases. As air passes up through a bed of particles, the relatively humidity (RH) of the air will increase until reaching 100%. At this point, no more drying is possible. The region between the upper boundary for dry particles to the point at which RH= 100% is called drying zone (Figure 2.6) (Bengtsson 2008). The thin-layer drying should not exceed the level where the air reaches 100% RH.

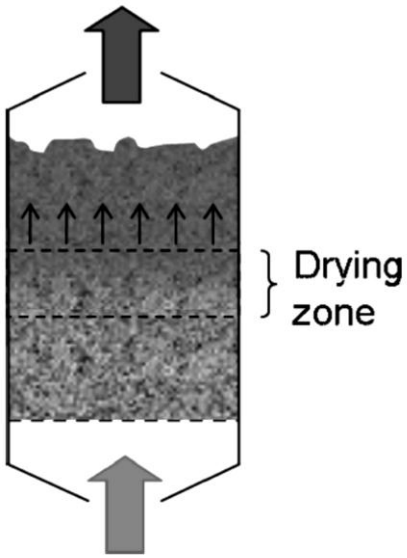

Figure 2.6 The drying zone progression through the bed material (Bengtsson 2008).

2.3.3.5 Furnish type

Logging slash, wood chips, and hog fuel are the three furnish types of wood residuals. The geometries of the three are different and there is no available research comparing how much the furnish type will affect the drying rate. For wood drying in general, drying rate is proportional to square root of thickness during the falling-rate period and inversely proportional during the constant rate period.

$$\frac{\text{Rate}_2}{\text{Rate}_1} = \left[\frac{\text{Thickness}_1}{\text{Thickness}_2}\right]^N \qquad \text{Equation 2-4}$$

$$\frac{\text{Time}_1}{\text{Time}_2} = \left[\frac{\text{Thickness}_1}{\text{Thickness}_2}\right]^N \qquad \text{Equation 2-5}$$

where N = 1, 2, or 1.5 (Mujumdar 1987).

2.3.4 Thin-layer dryer model description

Thin-layer dryer models are mostly used in food drying. The parameters are air velocity and drying temperature. Using experimental data, the researcher can estimate the effect of each parameter, then use these in a prediction model.

2.3.4.1 Available models to predict the drying curve

Some available models cited from Ertekin and Yaldiz's research are listed in Table 2.6 (Ertekin and Yaldiz 2004).

Table 2.6 Available models for thin-layer drying (Ertekin and Yaldiz 2004).

Mathematical models applied to drying curves

Model name	Model	Reference
Newton	$MR = \exp(-kt)$	Ayensu (1997), Hummedia and Sheikh (1989), Kassem (1998), Liu and Bakker-Arkema (1997), Nellist (1987), O'Callaghan, Menzies, and Bailey (1971), Sarsavadia, Sawhney, Pangavhane, and Singh (1999), Tiris, Ozbalta, Tiris, and Dincer (1994), Westerman, White, and Ross (1973)
Page	$MR = \exp(-kt^n)$	Agrawal and Singh (1977), Bruce (1985), Chhinnan (1984), Diamente and Munro (1993), Guarte (1996), Hutchinson and Otten (1982), Pathak, Agrawal, and Singh (1991), Sun and Woods (1994), Zhang and Litchfield (1991)
Modified Page	$MR = \exp[-(kt)^n]$	Overhults, White, Hamilton, and Ross (1973), White, Bridges, Loewer, and Ross (1978), White, Ross, and Ponelert (1981), Yaldız et al. (2001)
Modified Page	$MR = \exp[(-kt)^n]$	Overhults et al. (1973), Ozdemir and Devres (1999), Yaldız and Ertekin (2001)
Henderson and Pabis	$MR = a\exp(-kt)$	Bengtsson, Rahman, Stanley, and Perera (1998), Bhuyan and Prasad (1990), Chhinnan (1984), Guarte (1996), Pal and Chakraverty (1997), Rahman and Perera (1996), Rahman, Perera, and Thebaud (1998), Westerman et al. (1973), Yagcioglu et al. (1999)
Logaritmic	$MR = a\exp(-kt) + c$	Yagcioglu et al. (1999), Yaldız and Ertekin (2001)
Two term	$MR = a\exp(-k_0t) + b\exp(-k_1t)$	Henderson (1974), Madamba, Driscoll, and Buckle (1996), Rahman and Perera (1996), Rahman et al. (1998), Verma, Bucklin, Endan, and Wratten (1985)
Two term exponential	$MR = a\exp(-kt) + (1-a)\exp(-kat)$	Sharaf-Eldeen, Blaisdell, and Spagna (1980), Yaldız et al. (2001), Yaldız and Ertekin (2001)
Wang and Singh	$MR = 1 + at + bt^2$	Ozdemir and Devres (1999), Wang and Singh (1978)
Thompson	$t = a\ln(MR) + b[\ln(MR)]^2$	Paulsen and Thompson (1973), Thompson, Peart, and Foster (1968), Yaldız and Ertekin (2001)
Diffusion approximation	$MR = a\exp(-kt) + (1-a)\exp(-kbt)$	Kassem (1998), Yaldız and Ertekin (2001)
Verma et al.	$MR = a\exp(-kt) + (1-a)\exp(-gt)$	Verma et al. (1985), Yaldız and Ertekin (2001)
Modified Henderson and Pabis	$MR = a\exp(-kt) + b\exp(-gt) + c\exp(-ht)$	Karathanos (1999)
Midilli et al.	$MR = a\exp(-kt^n) + bt$	Midilli, Kucuk, and Yapar (2002)

Ertekin and Yaldiz (2004) stated that Midilli's model (Midilli 2002) was the best most fit the drying of eggplant, while Pardeshi, Arora et al. (2009) chose Thompson's model to be the best fit model during the drying of green peas (Pardeshi et al. 2009). The eggplant's final model is (Ertekin and Yaldiz 2004):

$$\mathrm{MR}=\frac{M}{M_0}=[a+b\ln(V)]\exp[-(cT^d)t^{(e+f\ln(V))}]+gt \qquad \text{Equation 2-6}$$

In equation 2-6, a, b, c, d, e, f, and g are constants. There is not a paper available to predict the drying curve using these models for drying biomass particles.

2.3.4.2 Primary criterion to select the best model

The root mean square error (RMSE) and coefficient of determination R-squared (R^2) are the most common primary criterion determining the goodness of the fit of model. When the data is not big enough, R^2 may not be as accurate as adjusted R^2. The adjusted R^2 increases only if the new parameter improves the model more than would be expected by chance and adjusted R^2 can be negative, and will always be less than or equal to R^2 (Wikipedia 2012). The best model has the highest R^2 and adjusted R^2, while the RMSE approaches to zero.

2.3.5 Deep bed drying analysis

Figure 2.7 shows characteristic functions of MC, drying rate, and temperature with time and Figure 2.8 shows the relationship between the moisture content and drying rate (Mujumdar 1987). From Figure 2.8, we can define several periods for deep bed drying. In the beginning of drying, the drying rate is increasing as the temperature is increasing. During the second period the drying rate is constant and the temperature is constant. Eventually the particle surface dried and in the third the drying rate is falling and temperature increases again.

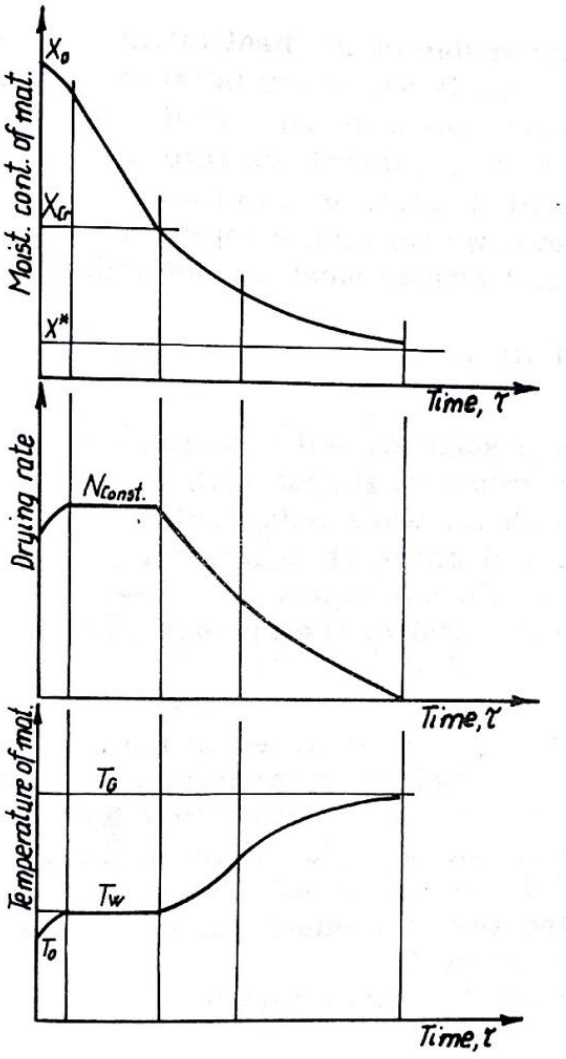

Figure 2.7 Drying characteristic functions of MC, drying rate and temperature with time (Mujumdar 1987).

Bengtsson (2008) showed for low-temperature bed drying with wood chips and sawdust that the constant-rate drying period was mainly affected by temperature and the falling-rate drying period was mainly affected by air velocity (Bengtsson 2008).

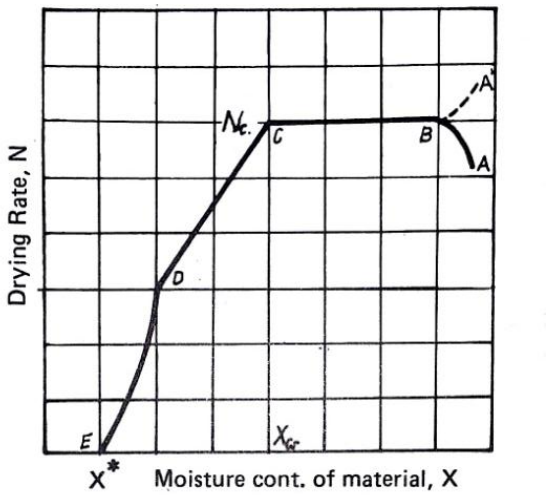

Figure 2.8 Drying rate curve with drying moisture content (Mujumdar 1987).

The drying zone is a region in which the actual drying takes place in a deep bed drying. Lerman and Wennberg's (2011) study on drying zone research shows that increasing drying temperature and air velocity will increase the drying zone velocity; increasing air velocity and height in the bed will increase the drying zone width (Lerman and Wennberg 2011).

Yrjola (2002) developed a deep bed drying model using aspen wood chips and compared the model with the experimental data as shown in Figure 2.9. The presence of a drying zone is demonstrated by the increase in temperature at different bed depths at different times.

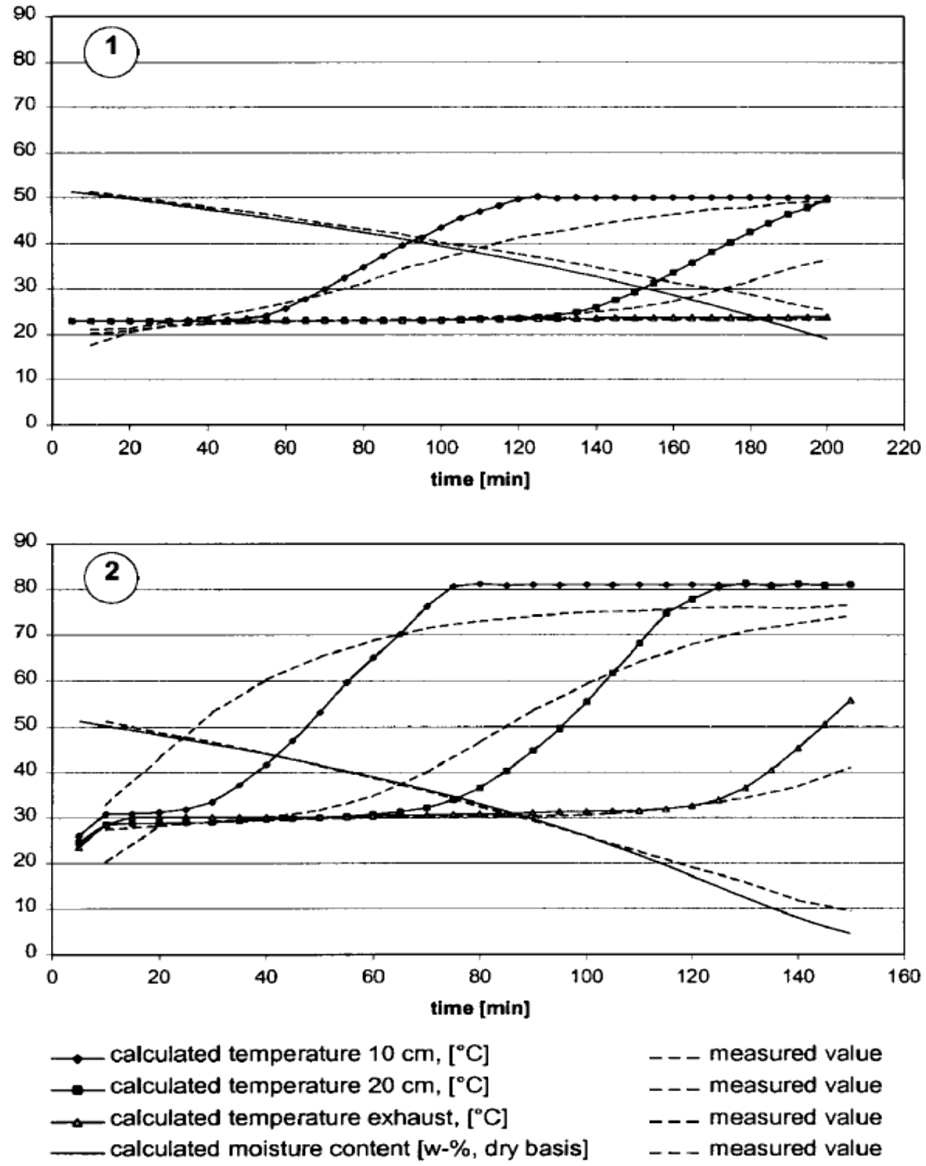

Figure 2.9 Comparison of measured and calculated values of moisture content for aspen chips (Yrjola 2002).

CHAPTER 3. Material and Methods

3.1 Material

The biomass used in this study was western hemlock (*Tsuga heterophylla*) and Douglas-fir (*Pseudotsuga menziesii*) wood chips supplied by Georgia Pacific Corporation, Philomath, OR. The chips were obtained on April 1 and May 3, 2011. The green material was sampled from outdoor storage piles. Care was taken to dig into the pile to avoid surface drying. The raw materials were shoveled into 20-gallon plastic containers prevent drying. To preserve freshness, the containers were either stored for up to two weeks in a cold room maintained at 5°C or frozen for longer term storage.

3.1.1 Particle size

Size distribution was determined using a 20”X50” oscillating shaker (Figure 3.1) with two screens. The top screen had 2” holes and the bottom screen had 3/8” holes.

Four containers of hemlock wood chips were randomly selected from wood collected during the second mill visit. The contents of each was weighed and poured onto the oscillating shaker individually. This yielded three fractions, -3/8”, +3/8”-2”, and +2”. Each fraction was weighed. The fraction weight was divided by the sum of the fraction weights to determine the percent of material in each fraction. The sum was also compared to the original weight in the container to

ensure that all material was accounted for. Average results of the three screenings are reported.

Figure 3.1 Oscillating shaker and wood chips on basket.

3.1.2 Initial moisture content

Four 120-g samples of wood chips were randomly picked from separate containers and were used to determine initial moisture content (MC_I) according to ASTM D4442. A sample was placed in a paper bag, sealed, weighed (W_I) on an Ohaus Voyager balance to 0.01 g, and dried for at least 24 hours in a Grieve oven at 103°C. The oven-dry samples were then weighed again (W_{OD}) within 30 seconds after being removed from the oven. Initial moisture content was calculated as:

$$MC_I = 100 \times \frac{W_I - W_{OD}}{W_{OD} - W_{Bag}} \qquad \text{Equation 3-1}$$

The average moisture content of the three samples is reported.

3.2 The drying equipment

An existing 40-cm-diameter bed dryer in the Department of Wood Science and Engineering at Oregon State University was used in this work. The dryer is direct-fired with natural gas and is capable of bed temperatures to 260°C and airflow to 3 m/s. The particle depth in the dryer can be up to 30.5 cm and the bed weight can be determined during operation.

3.2.1 Dryer gas supply

An overview of all equipment is given in Figure 3.2. Gas was supplied to the dryer from a New York Blower 1804S Pressure blower. The blower was rated at 0.19 m^3s^{-1} at 28 cm of water column and 204°C with a maximum temperature of 315°C. A Toshiba variable frequency drive allowed the blower to be operated at various speeds. A Power Flame FD75 natural gas burner controlled by a Honeywell Modutrol IV motor was located at the blower intake. Combustion gas from the burner was combined with ambient air and went to the blower intake through a 25.4-cm-diameter duct. The burner was a little oversized so that it was difficult to operate at low temperatures combined with low airflow without flameout (0.3 m/s in dryer and 50°C). Being oversize also caused control to be coarse. To get finer control (less valve movement for a given rotation of the control motor), the linkages were set for maximum mechanical advantage, one of two pathways through the control valve was sealed, and the gas supply pressure was reduced. This limited the upper end of the burner output to approximately 70%, but solved the control issues.

The gas exited the blower through a 15-cm diameter duct. The duct contained a Y connection in which manual dampers allowed the air to either go to the dryer or bypass the dryer. This allowed the burner and blower to run at a steady condition while the dryer was being loaded or unloaded. All ductwork was insulated with 5 cm of fiberglass.

At the base of the dryer the duct made a 90°turn and expanded to 46 cm. There were two perforated plates to make the airflow uniform across the bed cross section. The open area of the plates was 33%.

3.2.2 Dryer configuration

A photo of the dryer is shown in Figure 3.3A.The dryer walls are square in cross section, 56.5 cm on a side, and 125 cm high. The bottom of the dryer had a 46-cm-diameter hole to which the ductwork from the blower was attached. The top

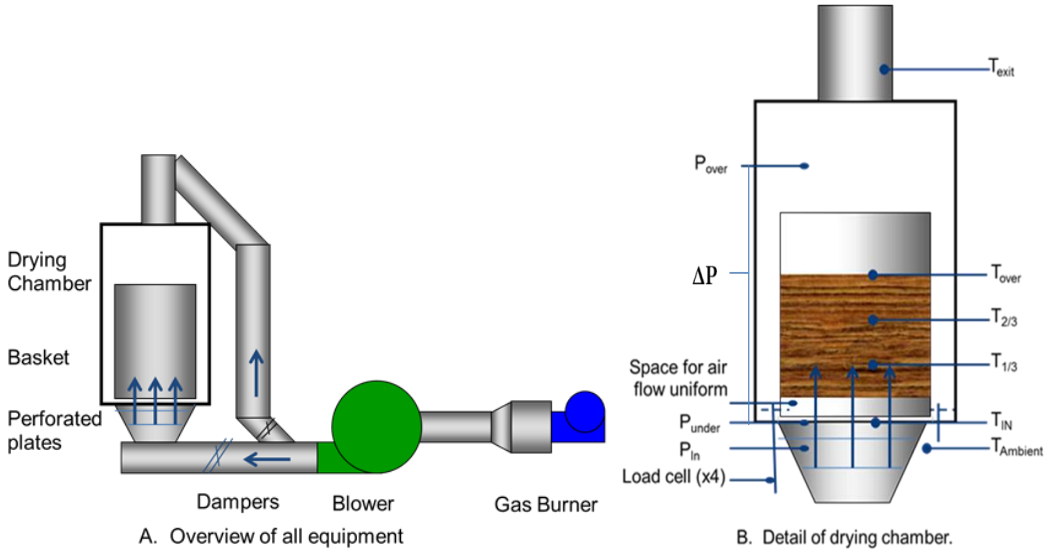

Figure 3.2 Experimental drying equipment.

of the dryer reduced to a 15 cm exhaust duct. There was a window through which the bed could be observed. The dryer was insulated with 5 cm of fiber glass. The front and back of the dryer were removable to allow access.

A 42 cm basket (Figure 3.2 b) was located in the dryer. It is 56 cm in height and constructed from 5.75 kg of aluminum to minimize its mass. The basket had a flexible gasket around its circumference at its base which touched the dryer structure and sealed the gap between the basket and the 46 cm hole at the bottom of the dryer structure. This ensured that the drying gas flowed from the duct into the basket and not around the basket. Care was taken in seal design so that the seal did not support the basket. To make the air flow uniform, the biomass material was raised from the bottom of the basket several cm by installing a screen to support the bed, as displayed in Figure 3.3 b. There are four ears with holes on the basket extending toward the four corners of the dryer. The basket was placed in the dryer so the holes in the ears rested on four rods. The rods passed through the base of the dryer to load cells. Thus, the basket could be easily removed, loaded or unloaded, and returned to the dryer. Nuts on the rods were used to do fine adjustment on the height of the basket (to make the seal work well) and to get the basket weight distributed on the four load cell rods. To get less heat leakage, the whole dryer was sealed as Figure 3.3B. A window was set into the wall to have a better view of drying process. Above the basket was 63cm of open space above which the dryer tapered to a 25cm duct. The duct took exhaust gases to a roof vent.

Figure 3.3 A. outside view of drying chamber drying chamber (left); B. inside view of drying chamber (right).

3.2.3 Instrumentation

Temperature was measured at several locations using type-T thermocouples. A thermocouple was located ahead of the blower to provide the blower inlet temperature to the control system. If the blower inlet exceeded 287°C the control system shut off the burner so the blower inlet gas remained below the maximum rated inlet temperature of 315°C. A thermocouple for the control loop that regulated the burner valve was located in the 15cm duct ahead of the Y and manual dampers. This was necessary so that a feedback signal was provided to the controller regardless of damper position. As displayed in Figure 3.2 b, two thermocouples were located directly under the perforated plate where the gas entered the dryer temperature (T_{in}). Three thermocouples were located in the dryer and could be positioned as needed. Generally one was placed directly above the

bed (T_{over}) and two were placed in the particle bed ($T_{1/3}$,$T_{2/3}$). Finally, a thermocouple was located in the duct leaving the dryer (T_{exit}).

Pressure was measured through taps in the dryer wall. Bulkhead fittings allowed tubes to be connected to pressure transducers on the outside of the dryer. Copper tubing was used on the inside of the dryer from the fitting to the location where pressure was to be measured. These locations were below the distributor plates (P_{in}), below the basket (P_{under}), and above the basket (P_{over}) as indicated in Figure 3.2 b. The pressure difference across the basket was a differential measurement. Other pressures were measured compared to atmospheric.

The weight of the basket was measured using four 9-kg load cells. The rods supporting the basket were connected to the load cells. Being outside the dryer, the load cells remained at near-ambient conditions and were not affected by dryer temperature. With periodic recalibration, the load cells recorded an initial weight that was within 2.5% of full scale. Recalibration was done with known weights up to 3 kg. The load cell readings were reduced when gas was flowing because the pressure was greater at the bottom of the basket. This error was corrected using the differential pressure measurement and the basket cross sectional area.

3.2.4 Control

The blower and burner were controlled via a computer using custom-written Labview software (Figure 3.4). Preliminary information, such as tare weight, data file name, dryer temperature, and blower speed, were entered. The user could then instruct the blower to turn on and activate the Honeywell ignition controller. Data

collection and control could be started and stopped independently. The data collection was set to 1.6 seconds. On the right of the operating panel in Figure 3.4, two graphs tell the operator the temperature and weight change trends during the drying. The figure to the lower left shows all the data in real time. Warning lights alert the operator to faults in the blower control, a flameout condition, or an over temperature condition to the blower.

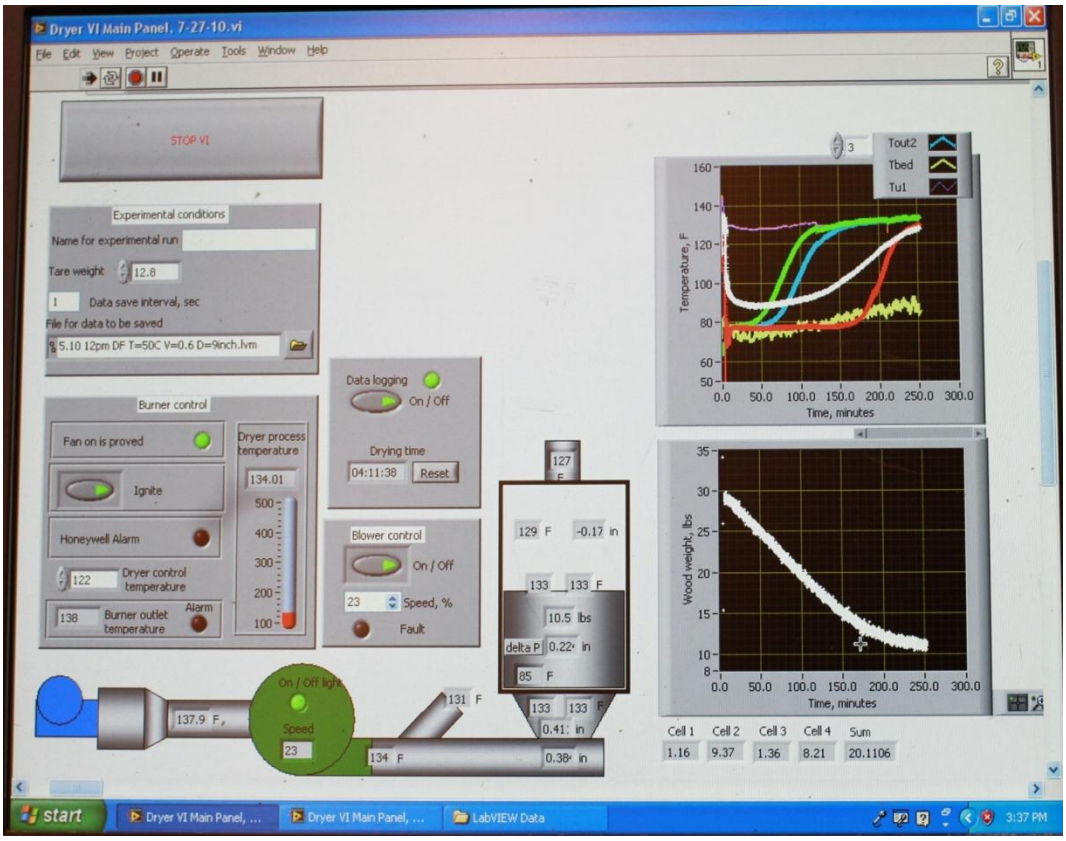

Figure 3.4 Labview operating panel.

3.3 Thin-layer experiments

Thin-layer drying experiments were done to determine drying curves for the material. The drying was conducted with approximately 1.3 cm of material in the bed. In this way there is little temperature change through the bed depth and it is assumed that all the material is exposed to the same temperature and the air humidity does not reach saturation. Drying curves were then constructed for a range of drying conditions based on the moisture content change versus time. The drying curves were then compared to several models in the literature to get an equation that best expressed the drying rate as a function of moisture content, gas temperature, and gas velocity. Two species and two particle sizes were measured, but the model was not extended to these.

3.3.1 Drying procedure

A 50-100 g sample of material to be dried was taken, placed in a paper bag, and weighed to 0.01g. It was then placed in an oven to determine initial moisture content by ASTM D4442. The dryer was brought to a steady state temperature with the empty basket in the dryer. The basket was then loaded with about 800 g of wood. The wood was spread uniformly so the depth was approximately 1.3 cm. At regular intervals a sample of about 50 g of material was removed from the bed and the material remaining in the bed releveled. The removed material was immediately placed in a paper bag, weighed, and placed in an oven to determine moisture content by ASTM D4442. The time intervals for sample collection ranged from 30 seconds to ten minutes depending on the dryer conditions and drying time. Samples were closely spaced in time early in drying and for high

temperature such as 200°C. Toward the end of drying and at lower temperatures the sampling interval was longer.

3.3.2 Experimental design

The conditions used in drying are shown in Table 3.1. The temperatures were 50°C, 100°C, 150°C, 200°C and the gas velocities were 0.3m/s, 0.6m/s and 0.85m/s. Temperatures were selected to represent the range that might be used industrially. Air velocities were less than 0.9 m/s because channeling and entrainment started to occur at this velocity. Three experiments were done at each condition. The first group of experiments was named group one. Two replications were done and were referred to as group two and group three. Occasionally a fourth replicate was done if there was a large difference in the drying curves in the first three runs. All of these were conducted with hemlock chips. The drying curves for Douglas-fir chips were compared to those for hemlock chips at the four conditions shown in Table 3.1. The effect of particle size was investigated with small (+3/8") particles, medium (-3/8"+2") particles and unscreened furnish. There were not enough large particles (-2") to test.

Table 3.1 Experimental design to determine the drying curves for the thin-layer drying.

	Drying air velocity (m/s)	Drying air temperature (°C)	Particle Size	Type of wood
Effect of drying air velocity and temperature	0.3	50	mixed	Hemlock
	0.3	100	mixed	Hemlock
	0.3	150	mixed	Hemlock
	0.3	200	mixed	Hemlock
	0.6	50	mixed	Hemlock
	0.6	100	mixed	Hemlock
	0.6	150	mixed	Hemlock
	0.6	200	mixed	Hemlock
	0.85	50	mixed	Hemlock
	0.85	100	mixed	Hemlock
	0.85	150	mixed	Hemlock
	0.85	200	mixed	Hemlock
Effect of particle size	0.6	150	Fine	Hemlock
	0.6	150	medium	Hemlock
	0.6	150	mixed	Hemlock
	0.85	100	Fine	Hemlock
	0.85	100	medium	Hemlock
	0.85	100	mixed	Hemlock
	0.3	200	Fine	Hemlock
	0.3	200	medium	Hemlock
	0.3	200	mixed	Hemlock
Effect of wood species	0.6	50	mixed	Douglas-fir
	0.85	100	mixed	Douglas-fir
	0.6	150	mixed	Douglas-fir
	0.3	200	mixed	Douglas-fir
	0.6	50	mixed	Hemlock
	0.85	100	mixed	Hemlock
	0.6	150	mixed	Hemlock
	0.3	200	mixed	Hemlock

3.3.3 Calculations to determine drying curve

The moisture content for the samples taken at time intervals was calculated using equation 3-2

$$MC = 100 \times \frac{W - W_{OD}}{W_{OD} - W_{Bag}} \qquad \text{Equation 3-2}$$

where W is the sample weight and W_{OD} is the oven-dry weight of the sample (both including bag weight, W_{Bag}).

The relative moisture content (MR) at each time interval was calculated using equation 3-3

$$MR = \frac{MC - EMC}{MC_I - EMC} \qquad \text{Equation 3-3}$$

where MC_I is the initial moisture content calculated by equation 3-1 and EMC is the equilibrium moisture content of the entering air. The equilibrium moisture content was determined using a stoichiometric calculation to determine gas humidity after the burner, the inlet temperature, and an EMC table (Forest Products Laboratory 2010).

3.3.4 Model development

A model was developed to predict the drying rate as a function of drying conditions. Using R and SAS statistical software, a simple model of the variables affecting the drying rate can be found and variables have significant effect on

drying rate determined. These variables included temperature, air velocity, furnish type. Table 2.6 shows 14 models developed for predicting the drying rate during thin-layer food drying. The experimental data from this study were fitted to all of these except Page model, two Modified Page model and Midilli et al.'s model. The best model was chosen for use in biomass drying. Root mean square error (RMSE) and adjusted R^2 (adj-R^2) were used as the primary criteria to select the best equation to account for variation in the drying rates of the dried samples.

The ten models were fitted by using time as the independent variable and MR as the dependent variable for each run and the adj-R^2 and RMSE were recorded. With the average of each model's adj-R^2 and RMSE, the results were compared among the models to determine the best model, one with the adj-R^2 approaching one and RMSE approaching zero. Fewer parameters were also considered a positive property of the best model.

After determining the best model, the next step was to get the best fit for the model coefficients as a function of temperature and air velocity. There are several steps to do this. First, the model was fit to for each experimental condition to get the actual coefficients as functions of temperature and gas velocity. Simple formulas were then used to fit the model coefficients to the drying conditions. We will get the best coefficient model by the same rule of adj-R^2 approaching one. Finally, using the drying model with the predicted coefficients, the drying at each condition was compared to the model to find the regions of good and poor

prediction. Some groups of graphs were made to visualize the difference between the predicted drying curve and the actual drying curve.

3.4 Deep-layer experiment

Deep bed experiments were conducted to verify the model developed using the thin-layer drying technique. Experiments were typically done with a 23-cm-deep bed, temperatures ranging from 50°C to 200 °C, and air velocities from 0.3 to 0.85 m/s.

3.4.1 Drying procedure

Load cell calibration was checked at the beginning of each experiment, the scale was tared with the empty basket, and the basket placed in the dryer. The dryer, including the basket, was preheated to a steady state condition matching the experiment to be done.

The initial moisture content (MC_I) of the material for each experiment was determined by randomly drawing three samples of 100–200 g from the container of material to be used for experiment. The samples were placed in separate paper bags, weighed, oven-dried by method ASTM D4442.

The airflow was set to bypass the dryer using the dampers on the Y in the dryer piping, the basket was removed, loaded, and weighed. If used, thermocouples were placed at 1/3 and 2/3 of the bed depth, 7.6 cm and 15.2 cm from the bottom of the basket. The material was leveled and the basket returned to the dryer. The difference between the sum of four load cells and the weight on the balance had to be less than 0.22 kg, otherwise load cells were recalibrated. The airflow was then redirected through the dryer, again using the dampers, to start the experiment. The Labview program recorded time, weight, temperature, and

pressure every 1.6 seconds and saved all data into a text file as indicated in Appendix 5. Other elements of the drying process, such as initial weights from the balance at start time, and the temperatures at the start time were manually recorded as shown in Appendix 4. As the rate of weight change approached zero and as the $T_{3/3}$ and T_{exit} approached the set point temperature, the heat was turned off. The basket was immediately removed, weighed, and the weight recorded as shown in Appendix 4. Three 500g samples were removed from the basket to determine final moisture content. The system then was allowed to cool for 5-10 minutes with air flow on.

3.4.2 Experimental design

The matrix of conditions tested was similar to those in the thin-layer experiments. The conditions used in drying are shown in Table 3.2. The temperatures were 50°C, 100°C, 150°C, 200°C and the velocities were 0.3m/s, 0.6m/s and 0.85 m/s. Temperatures were selected to represent the range that might be used industrially. Air velocities were less than 0.9 m/s because channeling and entrainment started to occur at this velocity. Two groups of experiments were done at each condition. The first group of experiments were named group one and the second repeat experiments named group two. Occasionally a third repeat experiment named group 3 was done if there was a difference in the drying curves in the first two runs. The groups in deep bed drying are separate from those in thin-layer drying. All conditions were used with hemlock chips and four conditions were used with Douglas-fir.

Table 3.2 Deep bed drying experimental design for factors effect on drying time.

	Drying air velocity (m/s)	Drying air temperature	Type of wood slash	Depth (inch)
Effect of drying air velocity and temperature	0.3	50	Hemlock	9
	0.3	100	Hemlock	9
	0.3	150	Hemlock	9
	0.6	50	Hemlock	9
	0.6	100	Hemlock	9
	0.6	150	Hemlock	9
	0.6	200	Hemlock	9
	0.9	50	Hemlock	9
	0.9	100	Hemlock	9
	0.9	150	Hemlock	9
	0.9	200	Hemlock	9
Effect of wood species	0.6	100	Douglas-fir	9
	0.6	100	Hemlock	9
	0.6	150	Douglas-fir	9
	0.6	150	Hemlock	9

3.4.3 Calculations

The deep layer bed drying lasted for hours in some cases so the 1.6 second data recording interval produced an unwieldy amount of data. Because the difference in the values recorded between adjacent intervals data is tiny, the data was averaged to 30-second intervals.

Moisture content was calculated from the raw weight data and graphs of MC and MR versus time were developed. All preheating (before material was added to the basket) data was dropped from further analysis and the time at which the basket was loaded into the dryer was set as time equals zero. Also, in some cases, the experiments were conducted longer than necessary to achieve dryness. In these cases unnecessary tailing data was removed. Also, the first few data points, taken as the airflow was started, were dropped from further calculations. The moisture content was calculated as

$$MC = 100 * \frac{\text{Total weight} - \text{Dry wood weight}}{\text{Dry wood weight}} \qquad \text{Equation 3-4}$$

where the weights are for the entire bed. MR was calculated in the same manner as thin-layer drying (Equation 3-3).

Moisture content and time were then used to calculate the drying rate for each time interval as

$$\text{Drying Rate} = \frac{\Delta MC}{\Delta t} \qquad \text{Equation 3-5}$$

CHAPTER 4. Result and Analysis

This chapter contains three sections: a description of the wood used, the thin-layer drying experiments, and the deep bed drying experiments. In addition, analysis and discussion of the results obtained in this project are presented in order to offer possible explanations.

4.1 Wood description

4.1.1 Size distribution

The hemlock chips were very uniform with 94.7% of the wood chips in the medium size class (+3/8,-2), 4.5% in the small (-3/8) size class and, 0.5% large particles (+2) (Table 4.1). The reason for the uniform size is that the wood chips were screened before we got them.

Table 4.1 Size distribution of hemlock chips.

wood chip				
Replicate	Sample g(%)	Small +3/8 g(%)	Medium (+3/8, -2) g(%)	Large +2 g(%)
No.1	15,100 (100)	740 (4.9)	14,270 (94.5)	40 (0.3)
No.2	17,780 (100)	800 (4.5)	16,880 (94.9)	70 (0.4)
No.3	18,490 (100)	810 (4.4)	17,540 (94.9)	130 (0.7)
No.4	19,270 (100)	850 (4.4)	18,240 (94.7)	128 (0.5)
Average Percent:	(100)	(4.5)	(94.7)	(0.5)

4.1.2 Initial moisture content

The average initial moisture content (MC_I) of wood was 159.8% (±2.3%) (Table 4.2). Thus, the variability of MC_I was small and could be considered as uniform for all the rest experiments.

Table 4.2 Initial moisture content of wood.

Initial MC	Sample			
No.	4	5	6	7
wet sample (g)	127.3	117.3	112.4	118.6
dry sample (g) (MC=4.21%)	51.7	47.4	44.4	47.2
dry sample MC=0 (%)	49.7	45.5	42.6	45.3
MC (%)	156.5	157.8	163.5	161.6
Average MC (%)	159.8			

4.2 Thin-layer drying

Figure 4.1 demonstrates the repeatability of an experiment done three times at the same conditions of temperature (50℃) and air velocity (0.6 m/s). The variability in moisture content among the experiments is acceptable.

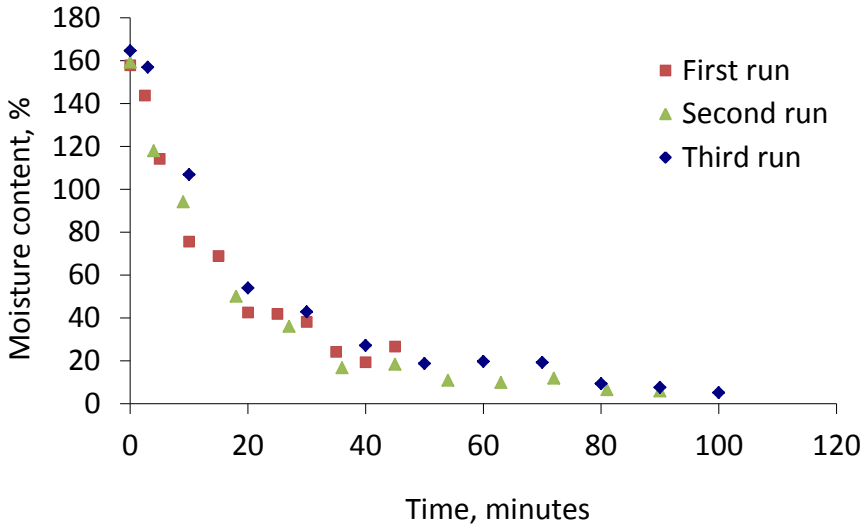

Figure 4.1 Three replicates of experiment data for hemlock at 50°C and 0.6 m/s.

4.2.1 Effect of Temperature

Figure 4.2 demonstrates a strong effect of temperature on the drying curve over the range of 50℃ to 200℃. Lines for higher temperatures appear lower in Figure 4.2. It appears that temperature has a greater effect at lower temperature than at higher temperature. The drying curve for T=50 ℃ is a large distance from the curve for T=100 ℃, while the drying curves for T=150 ℃ and 200 ℃ are near each other, or even hard to tell from each other. The reason can be explained by the movement of moisture internally is positively related to temperature (Mujumdar 1987). As calculated by Arrhenius relationship equation 2-2, the Arrhenius ratio is 5.2 between T=100 ℃ and T=50 ℃ while the Arrhenius ratio is only 2.7 between T=200 ℃ and T=150 ℃.

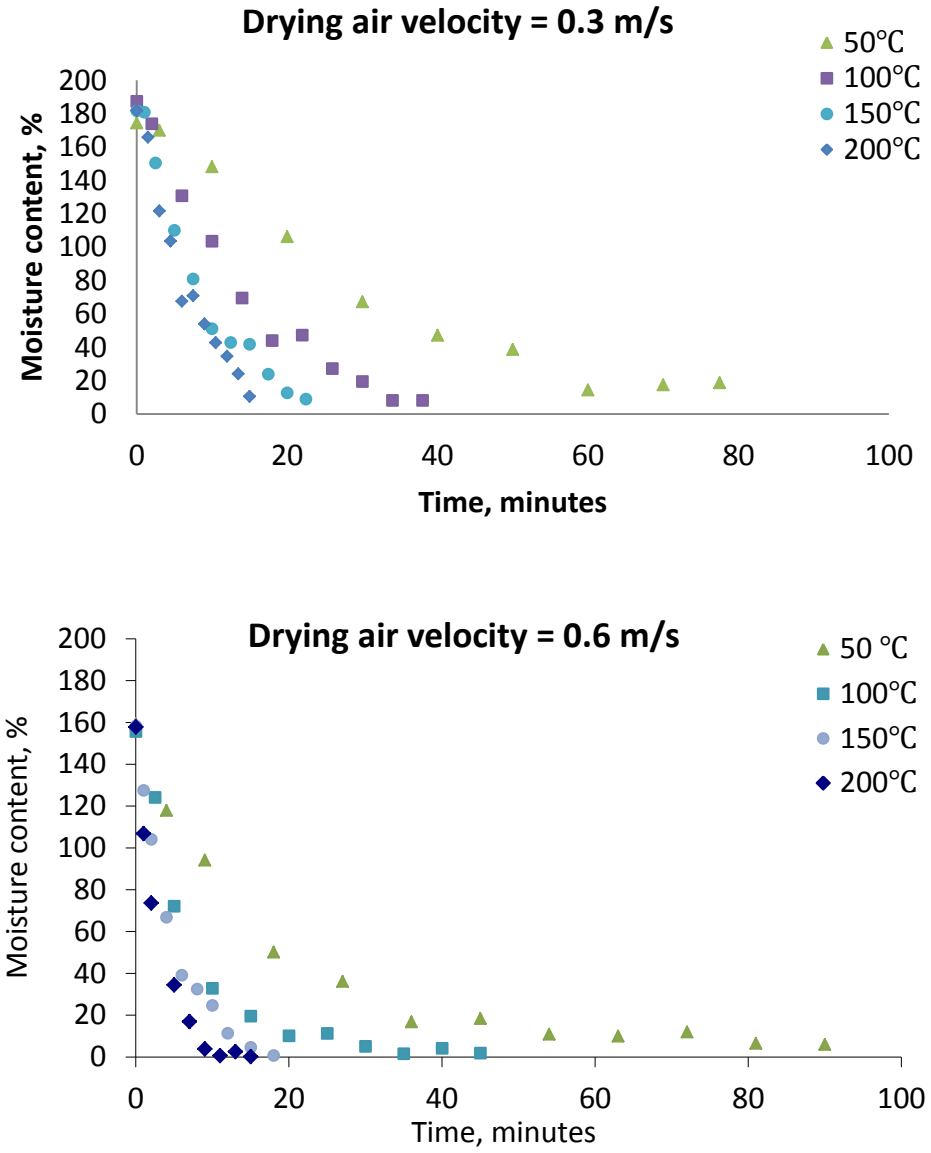

Figure 4.2 Effect of temperature on drying time in thin-layer drying.

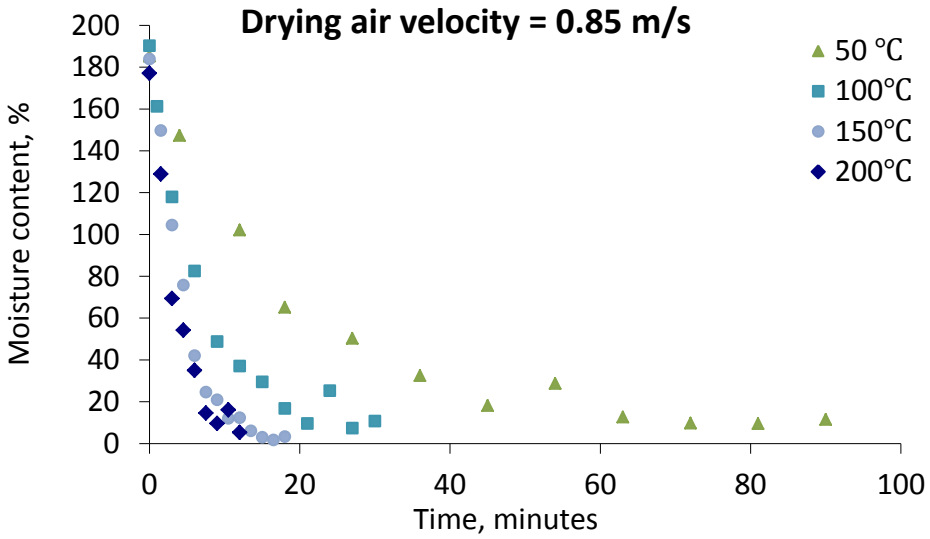

Figure 4.2 Effect of temperature on drying time in thin-layer drying (continued).

4.2.2 Effect of Velocity

A greater air velocity leads to a greater drying rate (Figure 4.3) at 100℃, 150 ℃, and 200 ℃ but the effect of velocity appears to be small at 50℃. Mujumdar (1987) indicates that air flow affects the drying rate by increasing convective heat transfer from the surrounding gas to evaporate surface moisture. This suggests that at 50°C the drying rate is limited by internal moisture movement. The particle temperature may reach the wet-bulb temperature and this controls the diffusion rate to the surface of the wood so that the drying rate does not increase at V= 0.6 m/s and 0.85m/s. This, however, does not fully explain the lack of a relationship between drying rate and air velocity at 50°C because increased heat transfer at the higher airflow should raise the particle temperature somewhat and increase the diffusion rate. It's possible that this effect is too small to be measured with the

experimental technique employed. At T=200 ℃ there is a large difference in the drying curves between V=0.3 m/s and V=0.6 m/s, while the difference is small between the V=0.6 m/s and V=0.85 m/s. At this high temperature it is likely that surface evaporation occurs rapidly and moisture movement is controlled internally, but the mechanism changes from diffusion to pressure-induced flow. That is, water boils inside the wood forcing the vapor to the surface of the wood. A higher airflow results in greater heat transfer and an increased drying rate. The drying rate change is greater between 0.3 and 0.6 m/s compared to 0.6 to 0.85 m/s. This agrees with theory shown in equation 2-1. The square root relationship suggests a 41% increase in rate as the air velocity changes from 0.3 to 0.6 and only a 19% increase between 0.6 and 0.85 m/s.

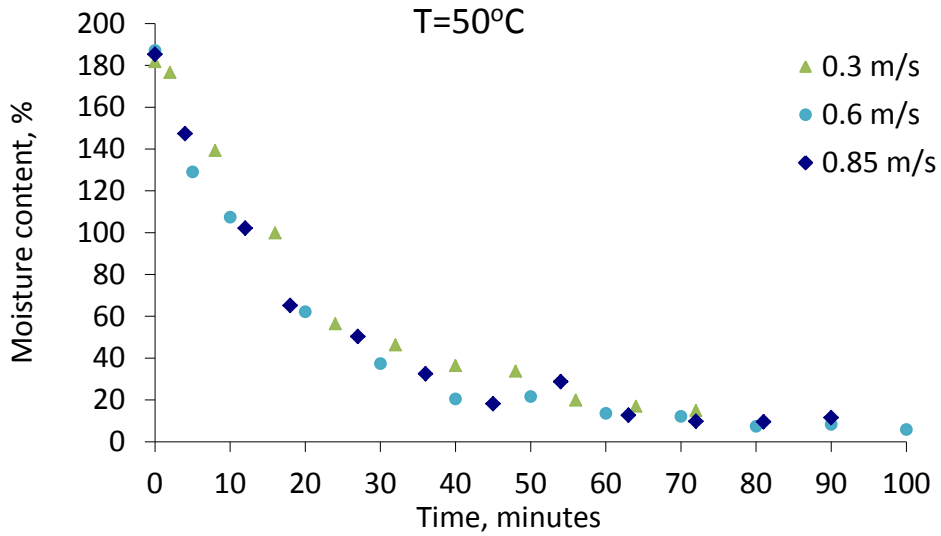

Figure 4.3 Effect of drying air velocity on drying time in thin-layer drying.

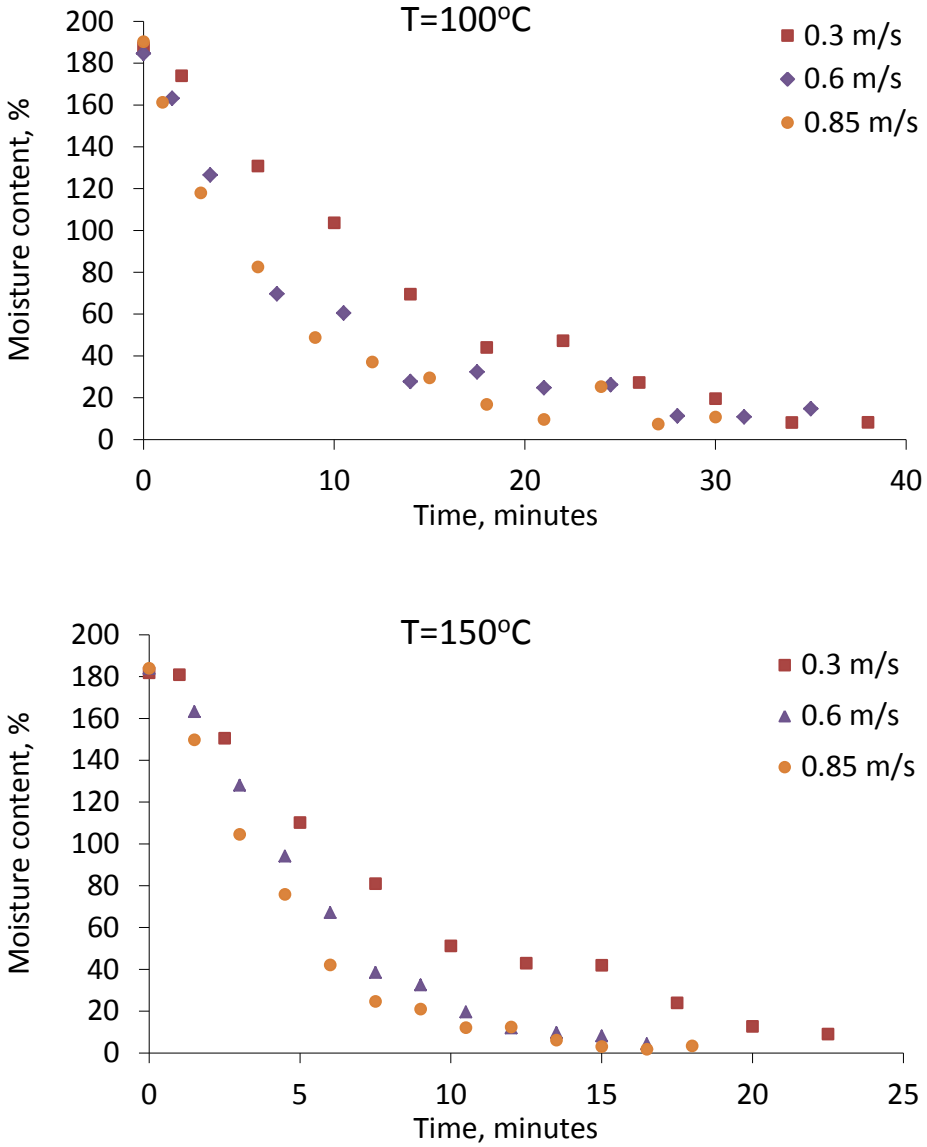

Figure 4.3 Effect of drying air velocity on drying time in thin-layer drying (continuted).

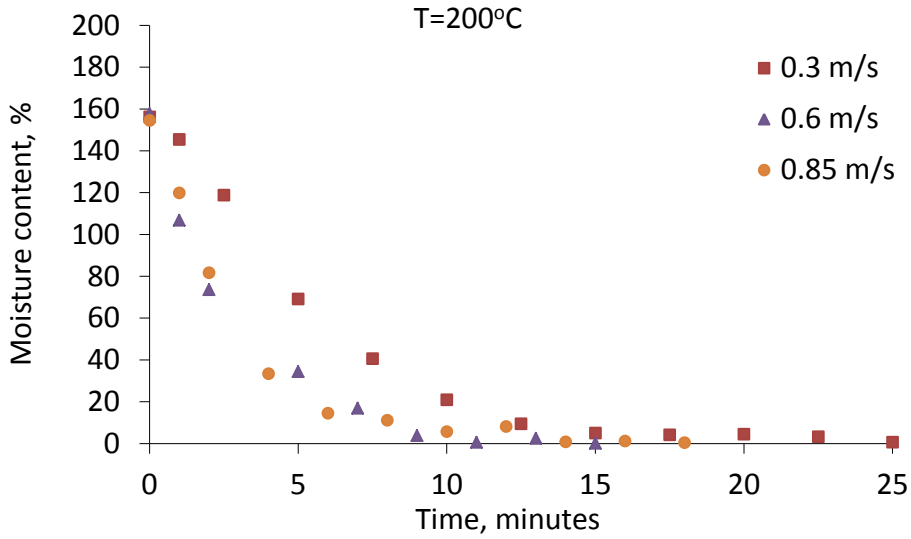

Figure 4.3 Effect of drying air velocity on drying time in thin-layer drying (continued).

4.2.3 Other effects

4.2.3.1 Particle size effect

Three experiments were done to compare the effect of particle size on drying behavior. As Figure 4.4 shows, at temperatures of 100℃ and 200℃, it is hard to see a difference between the drying curves for medium and fine particles. This result was unexpected and cannot be explained. Sampling may not have been properly done on the drying fine particle experiments. At temperature 150℃, the moisture content drops rapidly from 150% to 5% when drying fine particles. This would be expected given the larger specific surface areas associated with fine particles.

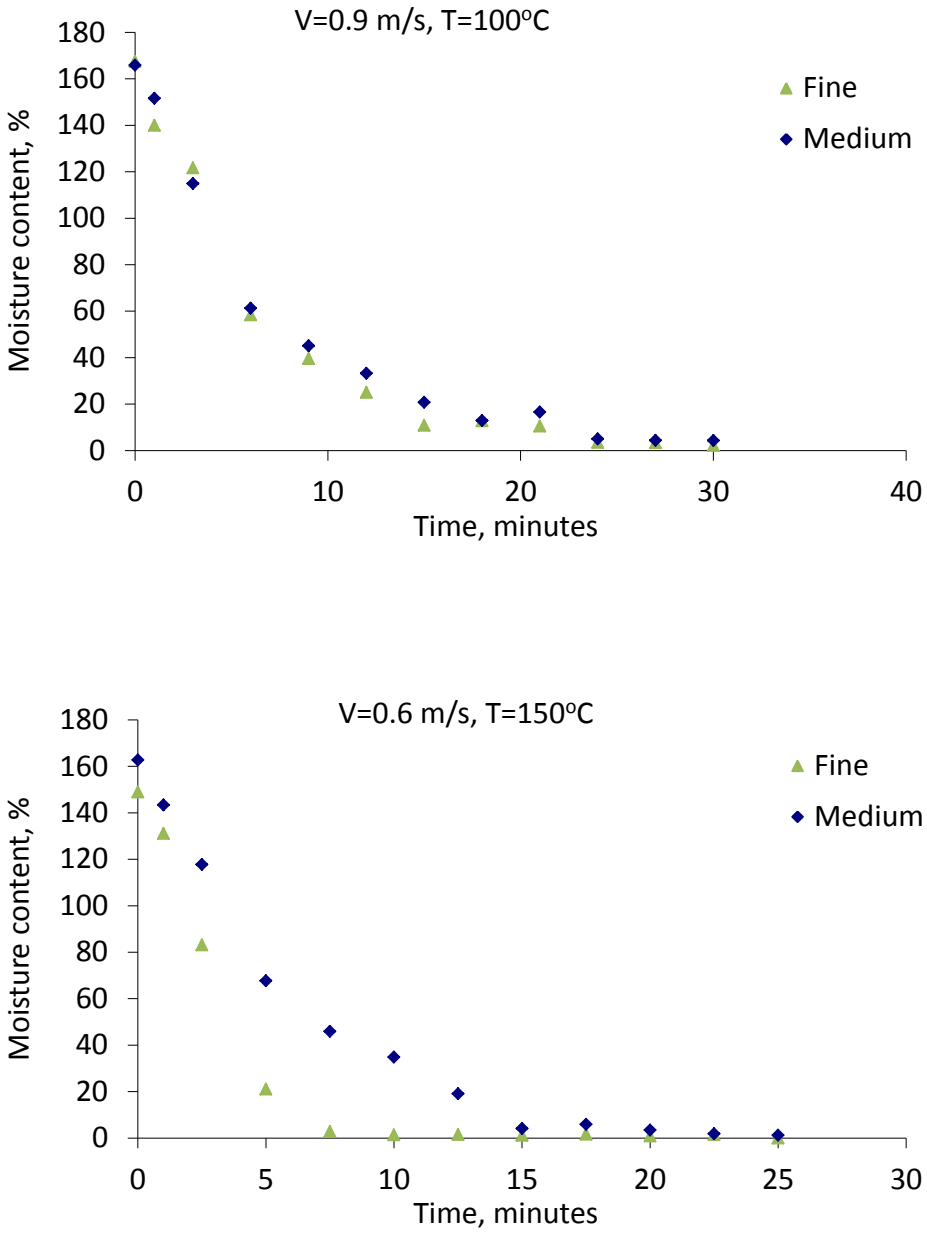

Figure 4.4 Effect of particle size at the same drying condition on drying time.

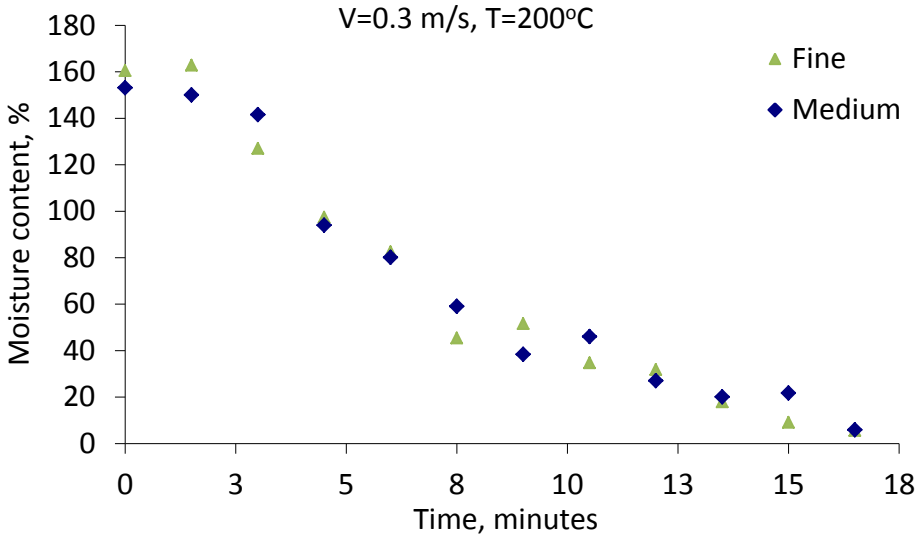

Figure 4.4 Effect of particle size at the same drying condition on drying time (continued).

4.2.3.2 Species effect

The moisture ratio is used instead of moisture content in this section to compare the drying of Douglas-fir and hemlock because of the large difference in the starting moisture content between the two species, around 95% and 160%, respectively. As indicated in Figure 4.5, the relative drying curves (MR) trends of Douglas-fir and hemlock are similar at a given condition of drying temperature and air velocity. No further conclusions will be made because each species would reach the same final moisture content at a different time given the difference in the initial moisture contents.

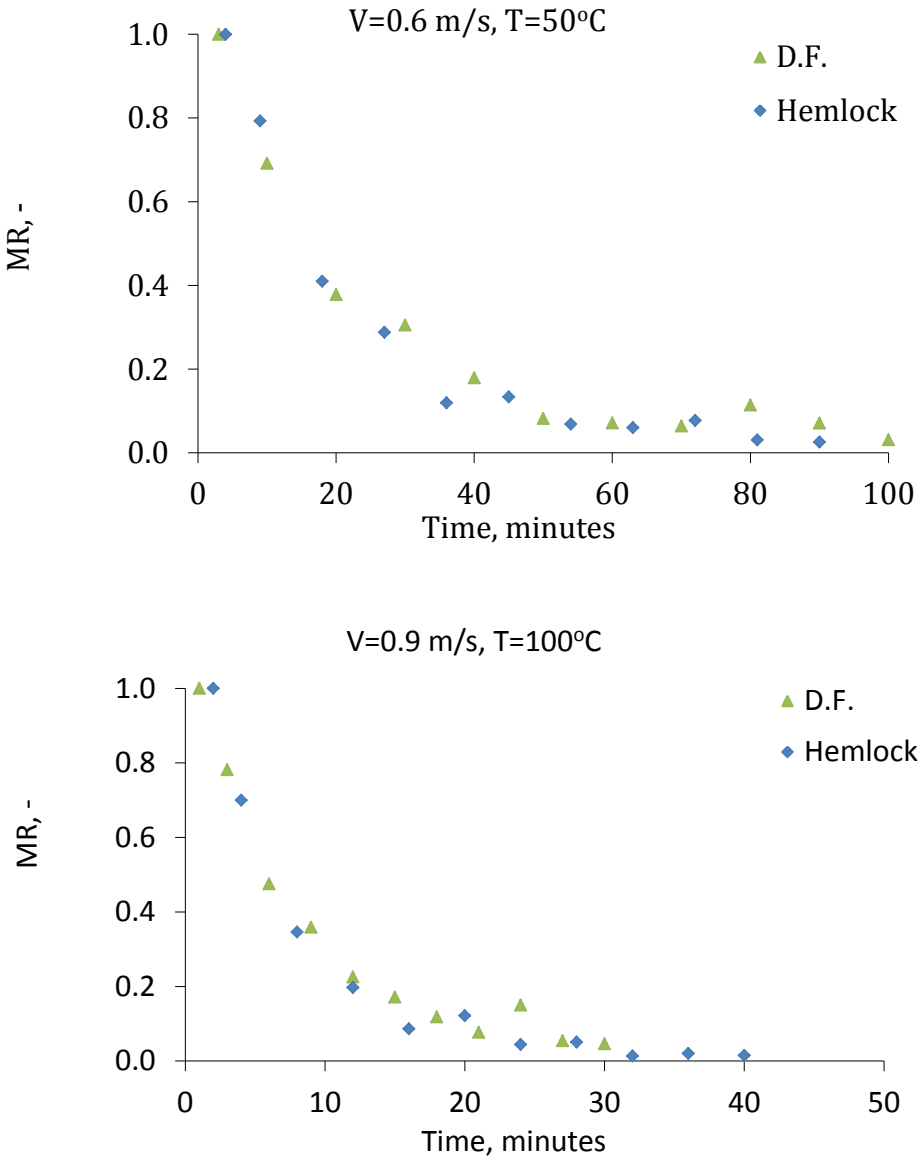

Figure 4.5 Moisture ratios versus drying time for different species at the same drying conditions. D.F. means Douglas-fir.

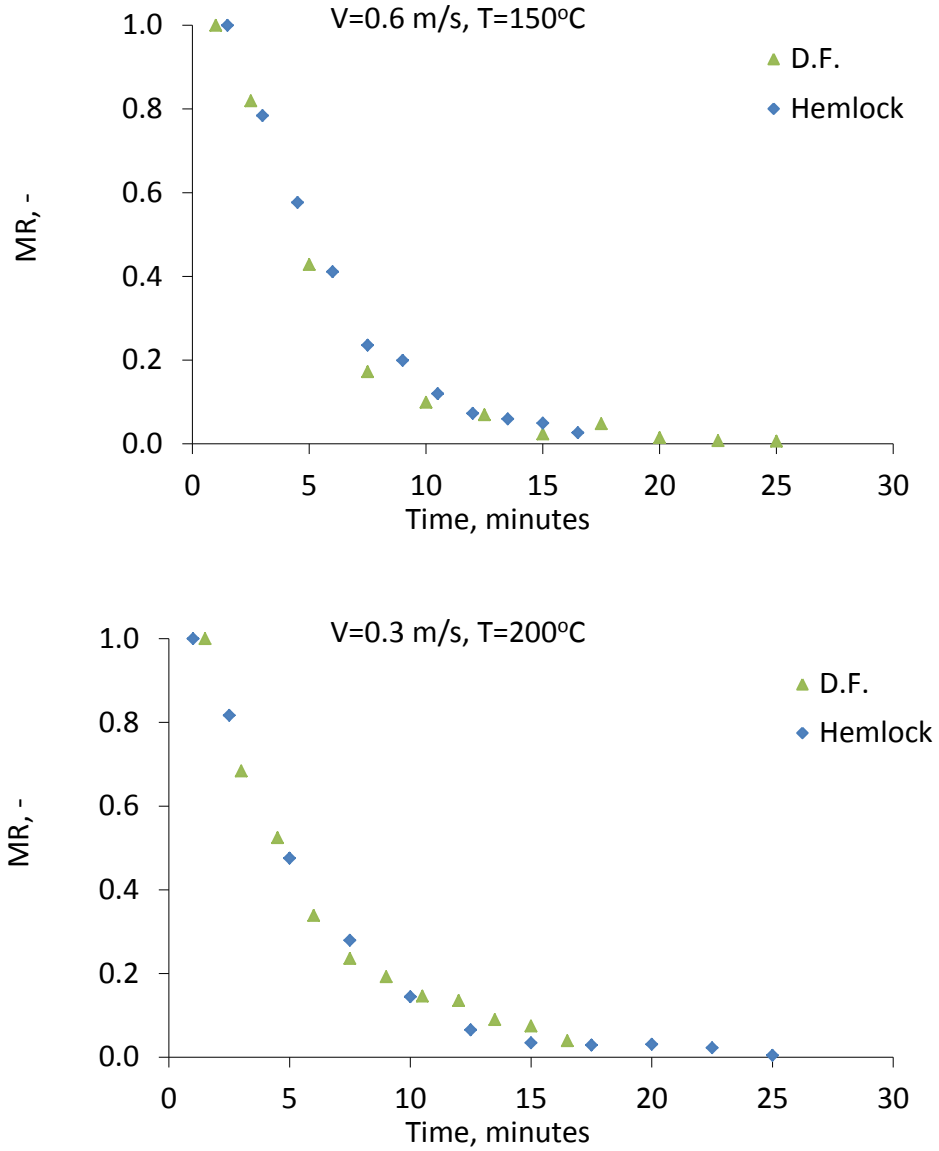

Figure 4.5 Moisture ratios versus drying time for different species at the same drying conditions. D.F. means Douglas-fir (continued).

4.2.4 Modeling thin layer drying

4.2.4.1 Thin-layer drying model

4.2.4.1.1 Model selection

The group two data was used to find the best model. Group two, the second replication of the thin layer experiment, had more uniform drying curves because of the experience gained when drying group one. Sample codes used for the regressions are shown in Appendix 2. SAS was used for eight models and R was used for two models as they are easy to fit. Each of the drying conditions for mixed hemlock particles in Table 3.1 was fit and these results are shown in Appendix 1. The average values of RMSE and adjusted R^2 from Appendix 1 are shown in Table 4.3.

From the Table 4.3 it can be seen that the Newton, Verma et al., and Modified Henderson and Pabis models generally work well (results in bold). The diffusion approximation model has negative value for the adjusted R-squared, which means the model doesn't fit. The Verma et al. model provides the best fit on this data. But considering that the Verma et al. model has three parameters and the Modified Henderson model has 6 parameters, the Newton model with one parameter was chosen. This is not only simple, but may be more robust than a multiparameter model. The model chosen in this study is Newton's model:

$$MR=e^{kt} \qquad \text{Equation 4-1}$$

Table 4.3 Statistical analysis results of the models by average RMSE and adjust R^2.

Statistical analysis for the models		
Model name	RMSE	adj-R^2
Newton	0.0602	0.9698
Henderson and Pabis	0.3169	0.1626
Logarithmic	0.2764	0.3631
Two term	0.3341	0.0696
Two term exponential	0.3169	0.1626
Diffusion approximation	0.4340	-0.5701
Verma et al.	0.0335	0.9906
Modified Henderson and Pabis	0.0380	0.9879
Wang and Singh	0.0599	0.9701
Thompson	1.5220	0.9208

This model is also consistent with drying theory for the falling rate period. Mujumdar (2007) suggests the following equation for food material

$$\frac{dMC}{dt} = k(MC - EMC) \qquad \text{Equation 4-2}$$

The solution of this has a form which matches the Newton model:

$$\frac{MC-EMC}{MC_i-EMC} = MR = e^{kt} \qquad \text{Equation 4-3}$$

4.2.4.1.2 Determination of model parameter

4.2.4.1.2.1 Fitting the model parameter k

The model parameter, k, in the Newton model is a function of the temperature and air velocity to which the particles are exposed. Table 4.4 shows the parameter k for each experimental condition. The actual temperature was 57℃ when the air velocity was 0.3 m/s because the burner could not be turned down further. Similarly, the actual temperature was 192℃ when air velocity was 0.9 m/s because the burner could not produce more heat.

Table 4.4 Values of k for each experiment.

		Temperature (℃)					
Velocity(m/s)	Group	50	57	100	150	192	200
0.3	1		-0.038	-0.110	-0.137		-0.214
	2		-0.038	-0.080	-0.163		-0.205
	3		-0.039	-0.089	-0.134		-0.154
	4						-0.174
0.6	1	-0.046		-0.115	-0.276		-0.442
	2	-0.041		-0.100	-0.252		-0.287
	3	-0.039		-0.077	-0.243		-0.252
	4						-0.332
0.9	1	-0.049		-0.124	-0.304	-0.311	
	2	-0.036		-0.112	-0.252	-0.456	
	3	-0.038		-0.100	-0.187	-0.283	
	4				-0.263	-0.336	

4.2.4.1.2.2 Table of the relationship between k and T and V.

The effect of temperature and air velocity on the drying coefficient k was analyzed for several equation forms using linear regression. The independent variables are temperature and air velocity and the dependent variable is k. The results are presented in Table 4.5.

Table 4.5 Parameter for k based on several models for temperature and air velocity.

NO.	Equation/ Model Parameter	R^2 (%)	RMSE
1	k= -exp(B/Temp)*A*SQRT(Vel)+C A= 11.46, B=-1583.41, C=.016	90.2	0.033
2	k= A*exp(-B/Temp) A= -4.24, B=1366.48	63.3	0.070
3	k= A*Temp^2+B*Vel+C A= 0, B= -0.15,C= 0.28	83.3	0.047
4	k= A*Temp+B*Vel+C*Temp*Vel A= 0, B= 0.91,C= -0.003	92.2	0.032
5	k= A*Temp+B*Vel+C A= -0.002, B= -0.15,C=0.62	84.0	0.046

The best fitting function and parameters occurred for model 4

k= A*Temp+B*Vel+C*Temp*Vel. Equation 4-4

However, based on the drying theory discussed in section 3.3 (Mujumdar 1987), the first model, with the second highest adjusted-R^2 and the second lowest RMSE, was chosen over the model 4. The model used to fit the parameter k is:

k= -exp(-1583.41/Temp)*11.46*sqrt(Vel)+.016 Equation 4-5

When this is substituted for k, the Newton model becomes:

MR=exp((-exp(-1583.41/Temp)*11.46*sqrt(Vel)+.016) Equation 4-6

This equation describes the drying behavior of the mixed hemlock particles when they are in contact with air of a certain temperature and velocity.

4.2.4.2 Comparison of the correlation to experiment data

Table 4.6 and Figure 4.6 show a comparison of the values for k fit directly from the experimental drying curves to the values for k predicted from equation 4-4. The average percent differences between these values at different drying conditions, shown in Table 4.7, indicate the model predicts k well at air velocities of 0.3 m/s and 0.6 m/s and also at 0.9 m/s if the temperature is high. The predictions were better at 100℃, 150℃, and 200℃ than at 50℃.

Figure 4.6 shows that the values for k for most experiments are near the line y=x, which means the model predicts k well. Two outliers ((200℃, 0.6 m/s in group 1) and (192℃, 0.9 m/s in group 2)) at the right of the figure may be caused by experiment operator error or other variability and a fourth replication at each of these conditions is included in the data. Figure 4.7 shows the predicted lines from equation 4.4 with the experimental data. It can be seen that Newton's model fits the thin-layer drying behavior of wood chips.

Table 4.6 Fitted and experimentally-determined values for k in the order of increasing temperature.

Exp.	Temperature	Velocity	Coefficient k		Diff.
			Experiment	Model	
	℃	m/s			%
1	56	0.3	-0.038	-0.035	9
2	56	0.3	-0.038	-0.035	8
3	57	0.3	-0.039	-0.036	8
4	50	0.6	-0.046	-0.050	-7
5	50	0.6	-0.041	-0.050	-22
6	50	0.6	-0.039	-0.050	-29
7	50	0.9	-0.049	-0.065	-31
8	50	0.9	-0.036	-0.065	-79
9	50	0.9	-0.038	-0.065	-31
10	100	0.3	-0.110	-0.074	33
11	100	0.3	-0.080	-0.074	8
12	100	0.3	-0.089	-0.074	17
13	100	0.6	-0.115	-0.111	3
14	100	0.6	-0.100	-0.111	-12
15	100	0.6	-0.077	-0.111	-44
16	100	0.9	-0.124	-0.140	-12
17	100	0.9	-0.112	-0.140	-25
18	100	0.9	-0.100	-0.140	-40
19	150	0.3	-0.137	-0.133	3
20	150	0.3	-0.163	-0.133	19
21	150	0.3	-0.134	-0.133	1
22	150	0.6	-0.276	-0.194	30
23	150	0.6	-0.252	-0.194	23
24	150	0.6	-0.243	-0.194	20
25	150	0.9	-0.304	-0.241	21
26	150	0.9	-0.252	-0.241	4
27	150	0.9	-0.187	-0.241	-29

Table 4.6 Fitted and experimentally-determined values for k in the order of increasing temperature. (Continued)

Exp.	Temperature	Velocity	Coefficient k		Diff.
			Experiment	Model	
	℃	m/s			%
28	150	0.9	-0.263	-0.241	8
29	200	0.3	-0.214	-0.205	4
30	200	0.3	-0.205	-0.205	0
31	200	0.3	-0.154	-0.205	-33
32	200	0.3	-0.174	-0.205	-17
33	200	0.6	-0.442	-0.296	33
34	200	0.6	-0.287	-0.296	-3
35	200	0.6	-0.252	-0.296	-17
36	200	0.6	-0.332	-0.296	11
37	200	0.9	-0.311	-0.366	-18
38	194	0.9	-0.456	-0.351	23
39	192	0.9	-0.283	-0.345	-22
40	192	0.9	-0.336	-0.345	-3

Table 4.7 Average difference percent between fitted and experimental-determined values for k.

	Temperature (℃)				
Velocity(m/s)	50	100	150	200	Average (%)
0.3	8	19	8	-12	6
0.6	-19	-18	24	6	-2
0.9	-47	-26	1	-5	-19
Average (%)	-19	-8	11	-4	

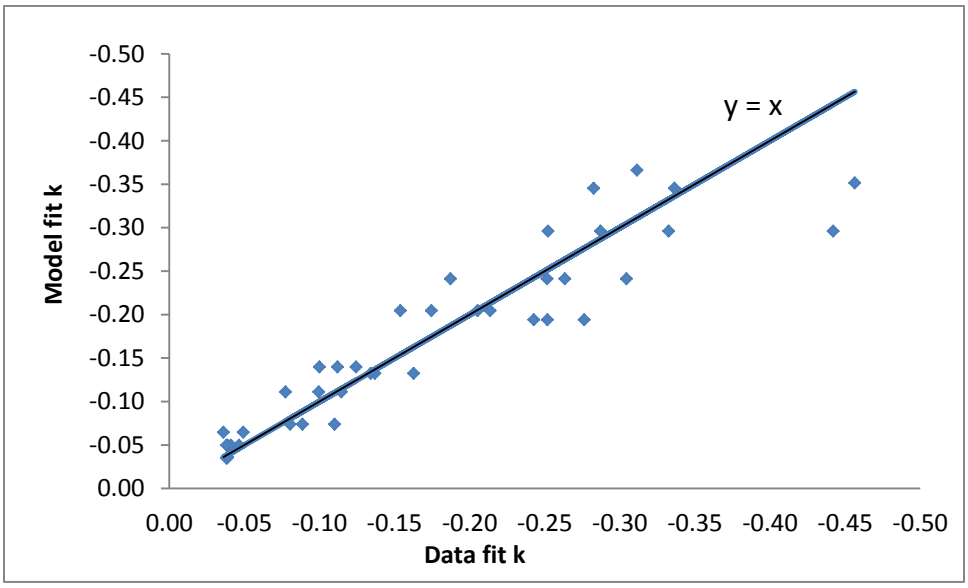

Figure 4.6 Comparison of the fitted parameter k (ordinate) to the experimental values (abscissa) for each experiment.

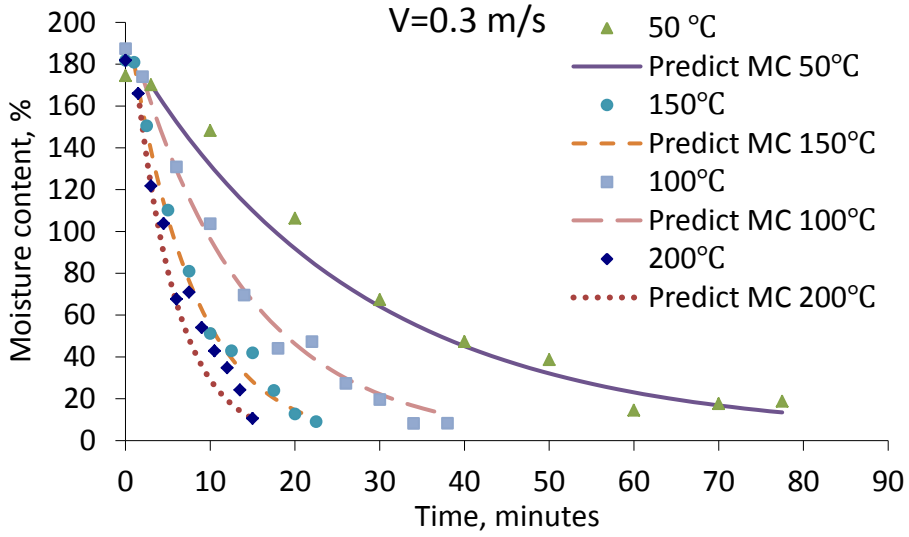

Figure 4.7 Predicted moisture content plotted with the experimental data for thin layer drying.

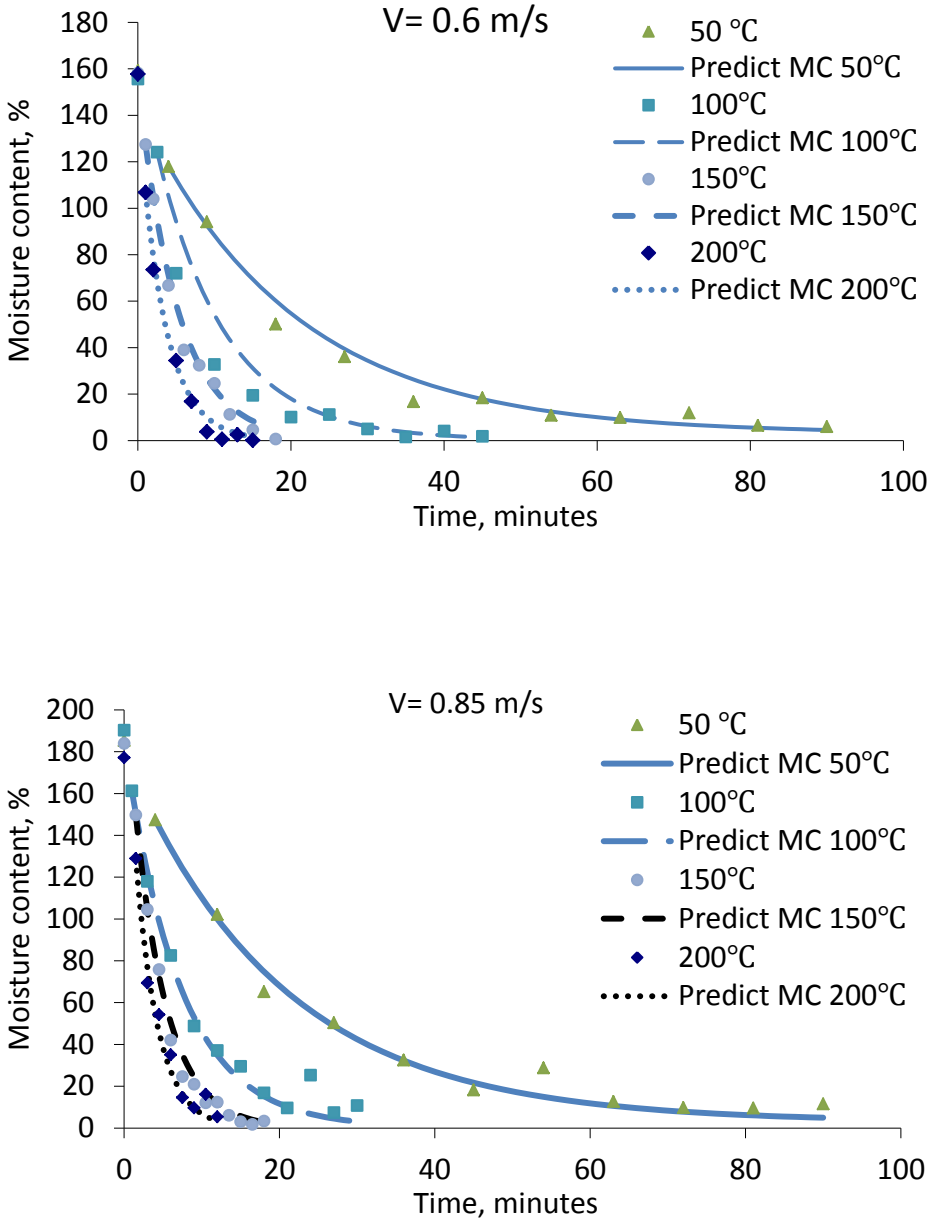

Figure 4.7 Predicted moisture content plotted with the experimental data for thin layer drying (continued).

4.3 Deep-bed drying

4.3.1 Experimental bed behavior

4.3.1.1 Load cell behavior

A typical deep-bed drying run is presented in this section. In this run, 28 lbs hemlock with 156% initial moisture content was dried at an air velocity of 0.3 m/s and temperature of 100℃ with a 23 cm bed depth.

The calculations of MC use the total weight data from the load cells. The load cell weight is affected by airflow. When the air flow is on, the pressure under the basket causes the sum of four load cells to be less than the actual weight. To obtain a corrected weight, a factor of 8.2 times $\Delta p+0.17$ was added to the load cell weight. The factor is derived from the area over which the pressure acts and the necessary unit conversions. The pressure drop across the basket was constant with time during an experiment.

Figure 4.8 shows the weight of wood decreasing with time and eventually approaching a constant weight at dryness. The line from load cells 1 and 3 are coincident, so only three load cell can be observed on the chart. On Figure 4.8, the total weight excludes tare weight of the basket, 12.7 lb. At the beginning of the drying some load cells show an increase in weight while others show a decrease. This is attributable to deformation in the metal basket at it heats. The total weight is unaffected by this.

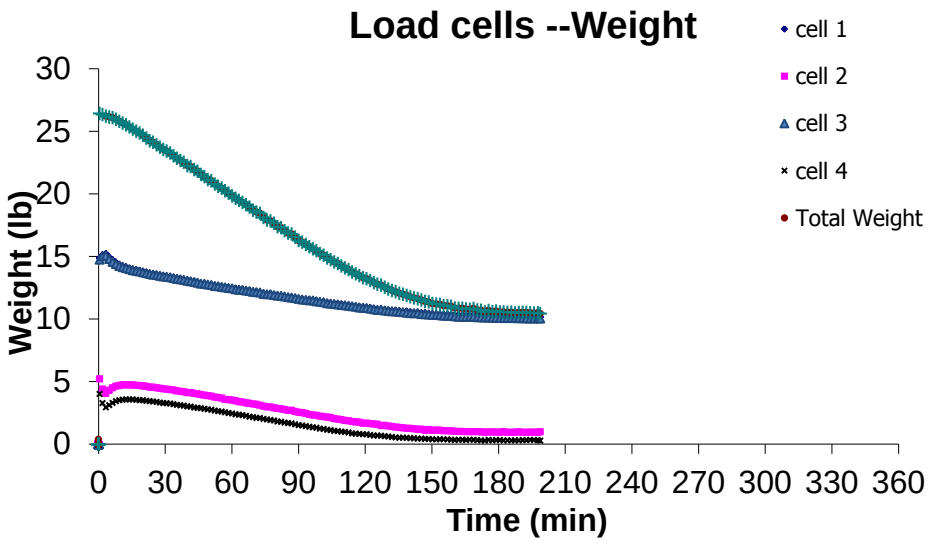

Figure 4.8 Load cell output and total weights versus drying time.

4.3.1.2 Moisture content versus drying time

Figure 4.9 shows the relationship between MC and drying time. There is a linear part from about 10 min to 120 min and nonlinear portions before and after that. The air leaving the bed is saturated during the linear period. The initial nonlinear period is due to heating of the material in the bed to the wet bulb temperature. After the linear portion the drying zone is at the top of the bed and air leaving the bed is not saturated.

4.3.2 Effect of drying parameters

4.3.2.1 Temperature

Figure 4.10 shows the temperature at six points in the dryer. T_{inlet} is the highest temperature and was measured below the distributor. $T_{1/3}$, $T_{2/3}$, and $T_{3/3}$ are the temperatures of sensor at depth of 7.5, 15, and 23 cm, respectively,

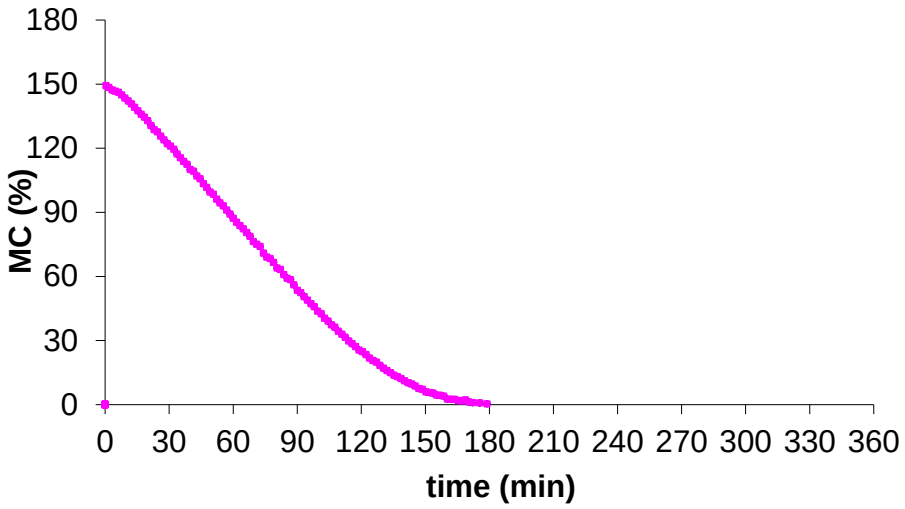

Figure 4.9 Average bed moisture content versus time for deep bed drying.

corresponding to 1/3 of the bed depth, 2/3 of the bed depth, and the surface of the bed. Initially, these temperatures are near the wet-bulb temperature and after the particles dry at a given location they are near the inlet temperature. They provide information about the location, thickness, and velocity of the drying zone. $T_{ambient}$ is the lowest temperature and was measured outside the dryer near the load cells. It was used to verify that the load cells' temperatures were stable. T_{exit} is measured at the dryer exit and is initially greater than the bed exit temperature ($T_{3/3}$) because

some air passes around the basket and because the dryer was preheated to the dry-bulb temperature. It is lower than $T_{3/3}$ at the end of drying, probably due to heat losses through the dryer walls.

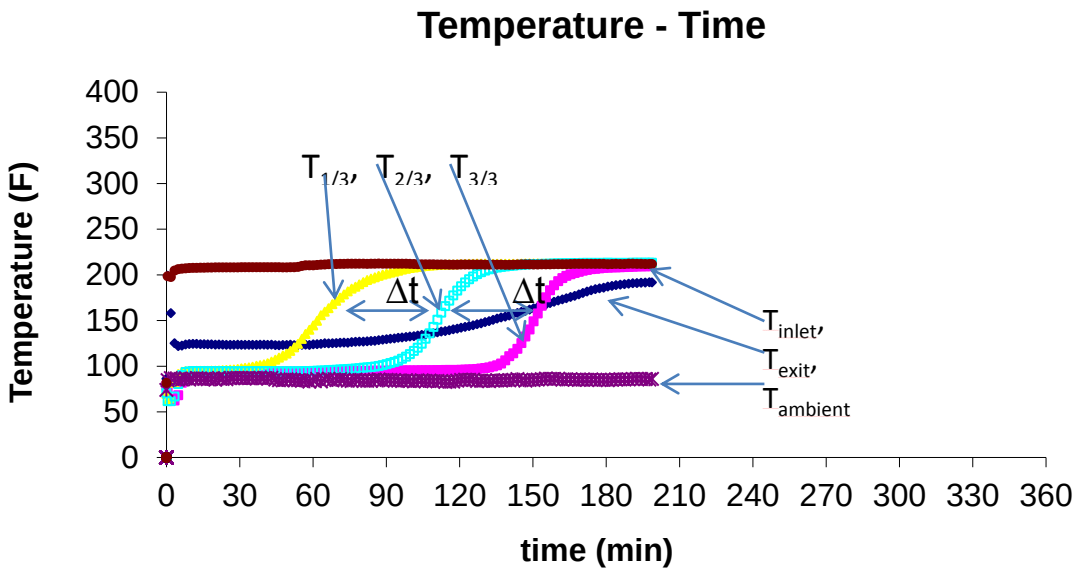

Figure 4.10 Temperatures at six bed and dryer locations versus drying time.

Figure 4.11 shows the temperature effect on drying time with different air velocities. All the data in these graphs is from the Group 1 experiments. As expected, temperature strongly affects the drying rate. Much of this effect is because warmer air entering the dryer can carry more water with it because it

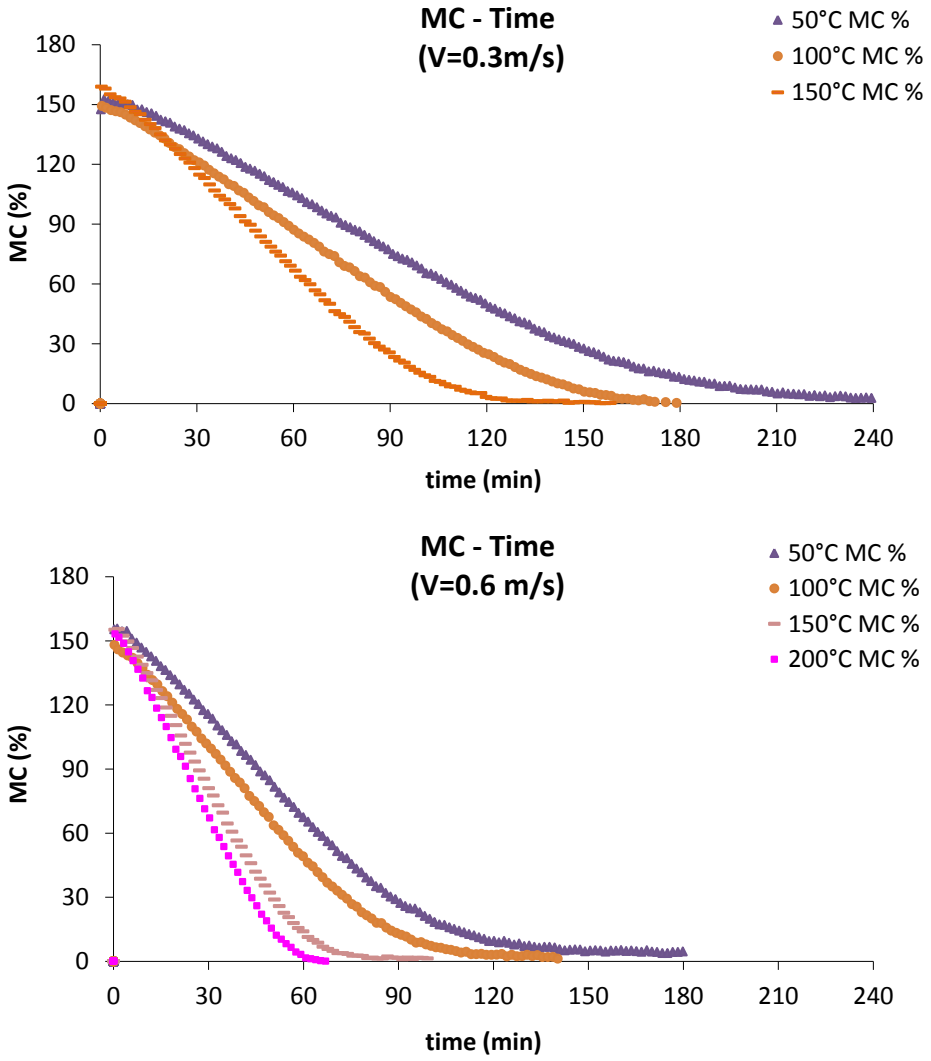

Figure 4.11 Effect of drying air temperature on drying time in deep bed drying.

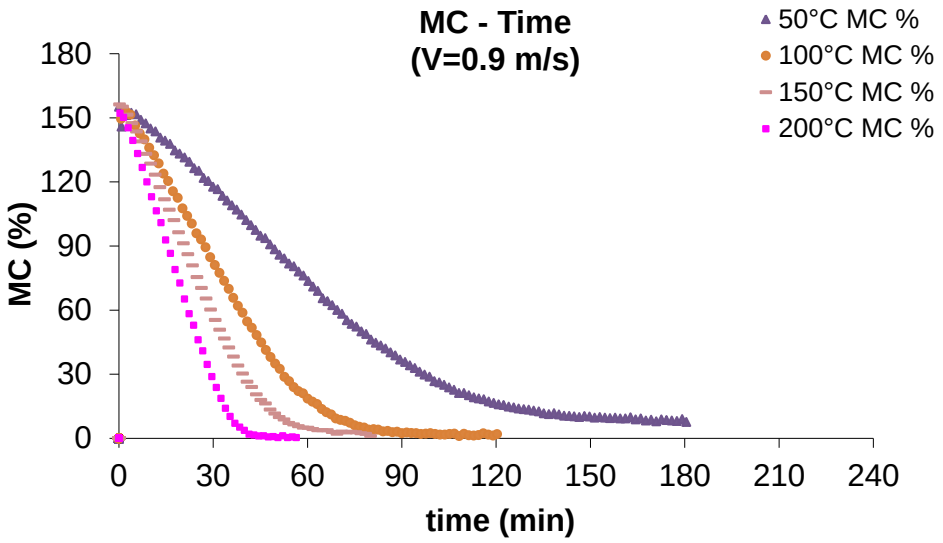

Figure 4.11 Effect of air temperature on drying time in deep bed drying (continued).

leaves the dryer at a higher temperature. The temperature entering the bed may be limited to about 200℃ because it was observed that some wood particles changed to a dark color when the average MC approached zero.

4.3.2.2 Air velocity

Figure 4.12 shows the effect of air velocity on drying time at different drying temperatures. The data in these graphs is from the group two experiments. As expected, air velocity is another key parameter that strongly impacts the drying rate. Again, the air leaves the bed saturated and if the airflow is greater then the mass flow of air is greater and it can carry more water out of the bed. The air

velocity was limited to less than 0.9 m/s to avoid particle entrainment. This value would vary with particle size.

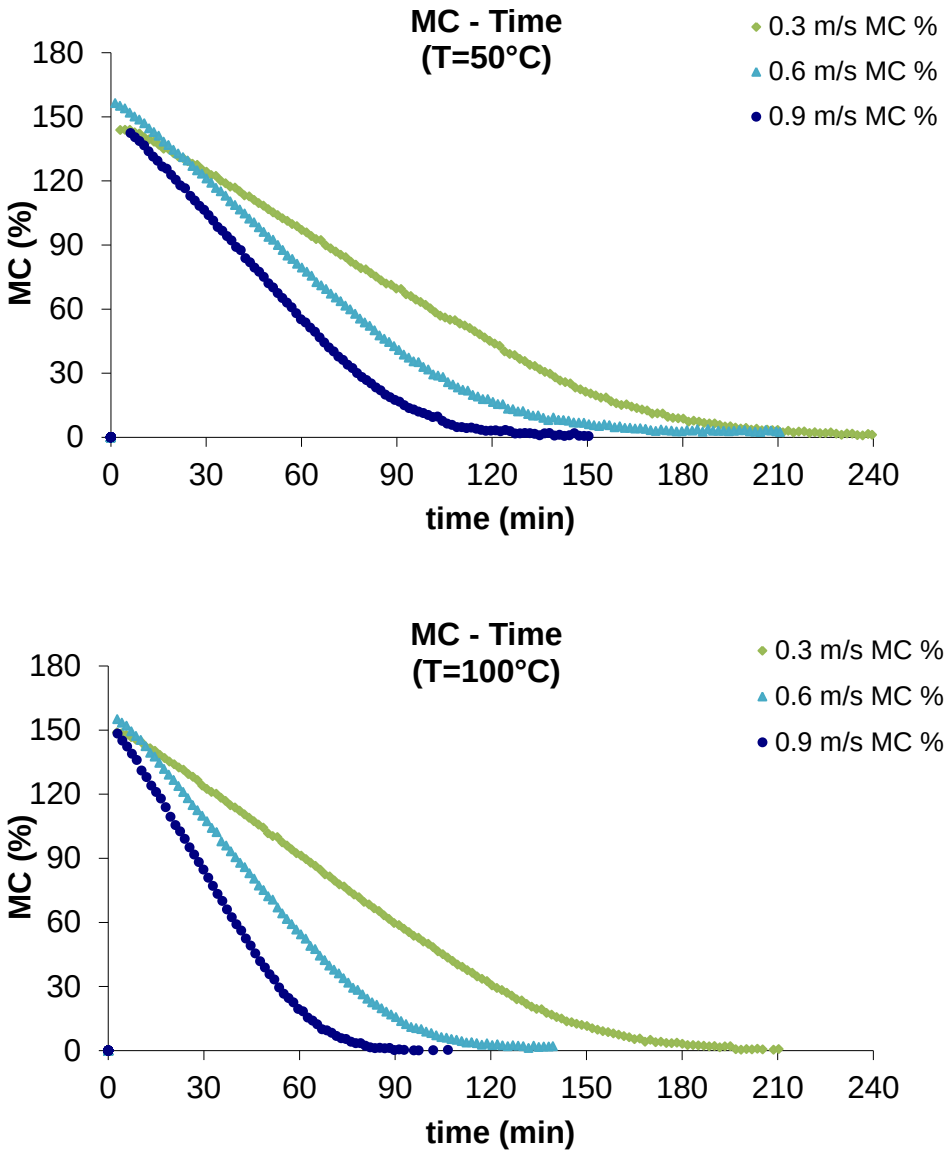

Figure 4.12 Effect of air velocity on drying time in deep bed drying.

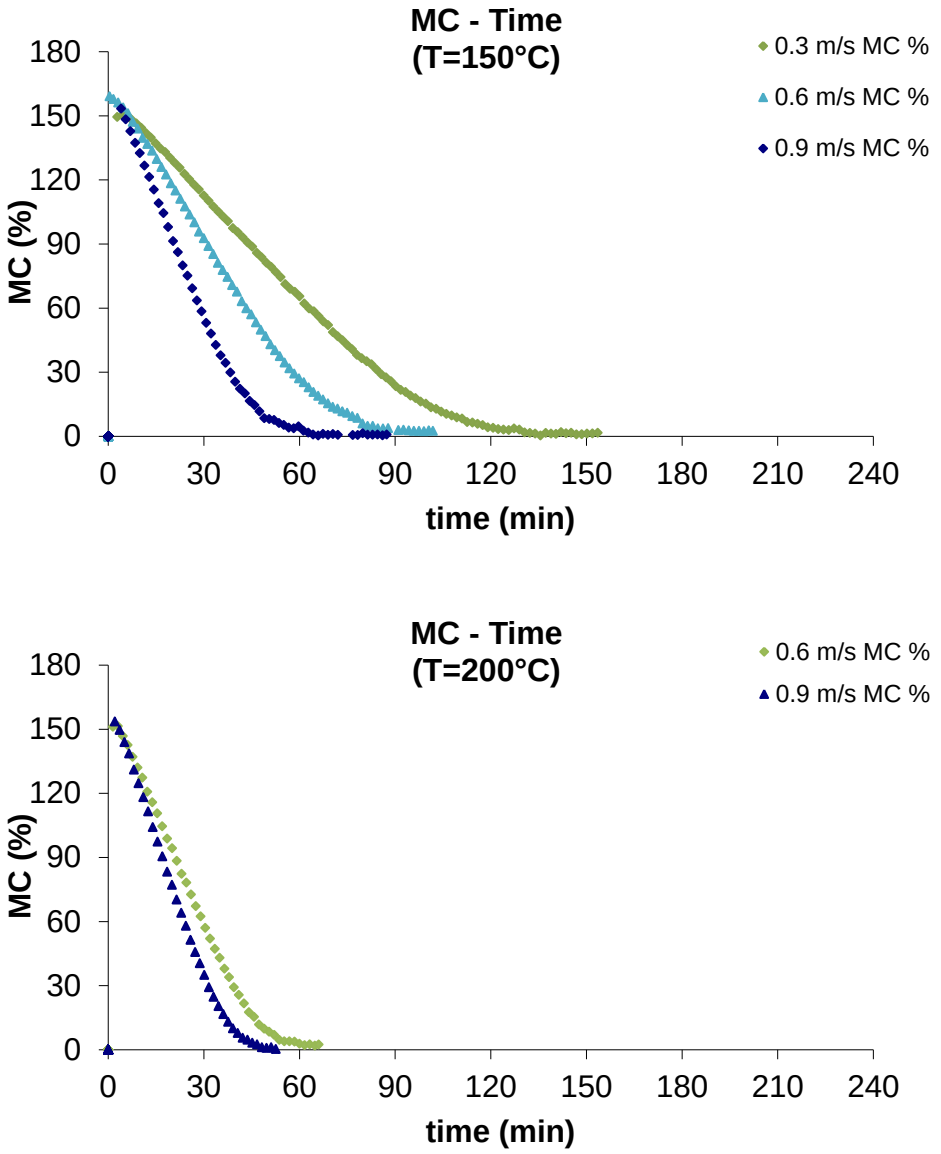

Figure 4.12 Effect of drying air velocity on drying time in deep bed drying (continued).

4.3.2.3 Species effect

Figure 4.13 indicates that the drying curves are not similar for Douglas-fir and hemlock. One would not expect them to be because drying is limited by the

ability of the air to remove water from the bed (it leaves saturated) and hemlock contains significantly more water (150%) compared to Douglas-fir (95%). One would therefore expect a longer drying time for hemlock. As indicated in Figure 4.14, the drying rates are almost the same at the same MC between the Douglas-fir and hemlock. At high moisture content the water removal rate from the bed determines the rate (assuming similar dry bulk densities). At low moisture content the reason may explained by species effect being small in drying wood particles of these two species..

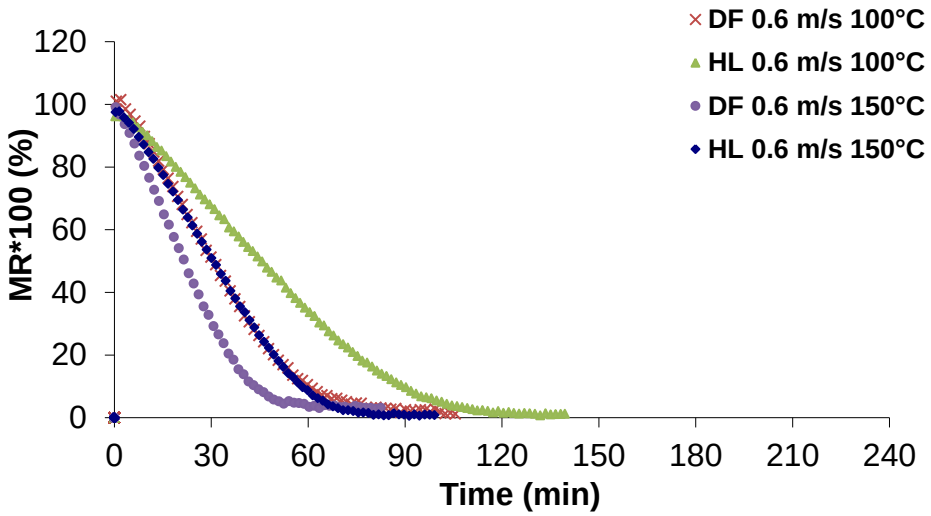

Figure 4.13 Drying comparisons of Douglas-fir and hemlock by moisture ratio.

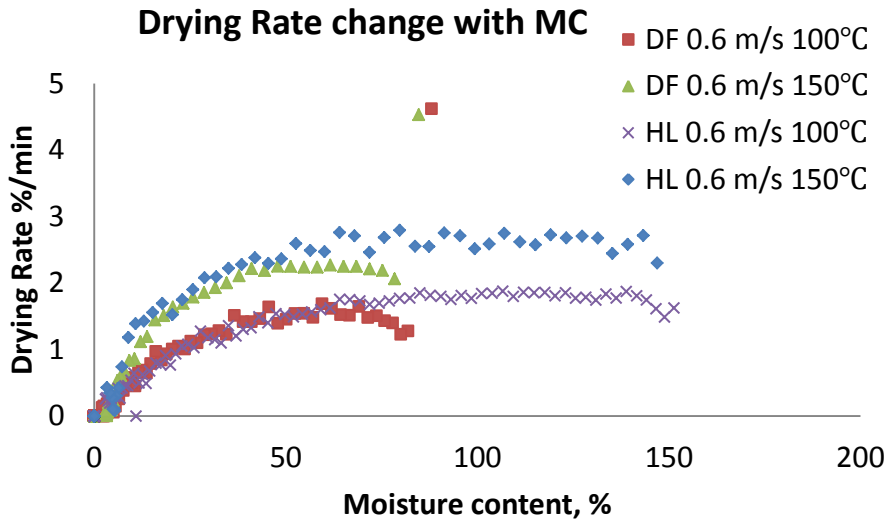

Figure 4.14 Drying comparisons of Douglas-fir and hemlock by drying rate.

4.3.3 Drying rate and drying zone

4.3.3.1 Drying rate

Figure 4.15a and 4.15b show the drying rate as a function of time and moisture content, respectively. The line in Figure 4.15a can be divided into four parts. The first part is heating period (0-10 min, MC% 145-150%) during which the drying rate is increasing to a constant level. The second part is constant rate drying (10-100min, MC% 50-145%) during which the drying zone is fully inside the bed. This is the most efficient stage of drying. The third part is a falling period (100-180 min, MC% 0-50%) during which the upper bound of drying zone is moving out of the bed and the lower bound is still inside and moving upwards. The air leaving the bed is not saturated and the drying efficiency is decreasing. The last stage is the top layer drying period (180 min- end, MC approaching to 0). The drying process

has mainly ended, only a few top layers may still be drying, and the efficiency is approaching zero. The drying process should be stopped prior to this stage.

As discussion in section 2.3.3.1, it was uncertain whether the air velocity affects drying rate in falling rate period or not. Mujumdar (1987) states that air velocity has no effect on falling rate period drying in lumber drying while Bengtsson (2008) stated that decreasing air velocity increased the falling rate period in drying wood chips. From the data and graphs in this study, the drying rate during the falling rate period is not strongly affected by air velocity. If the nonlinear tails (falling rate periods) in Figure 4.12 are shifted so the lines overlap, there appears to be little difference in the shape of the curves or the duration of the constant rate period. At the end of the linear portion of these curves, the drying zone has reached the top of the bed and is moving out of it. Some particles may still be experiencing constant rate drying and their drying rate is affected by velocity.

In Figure 4.15b, the drying rate from Figure 4.15a is expressed as a function of moisture content. At the point MC = 0% (circled in Figure 4.15b), the drying rate decreases rapidly and approaches zero as the moisture content approached the equilibrium moisture content. If there is thermal degradation of the wood at this point, the volatile organic compounds lost would appear as moisture in the weight loss and subsequent calculation.

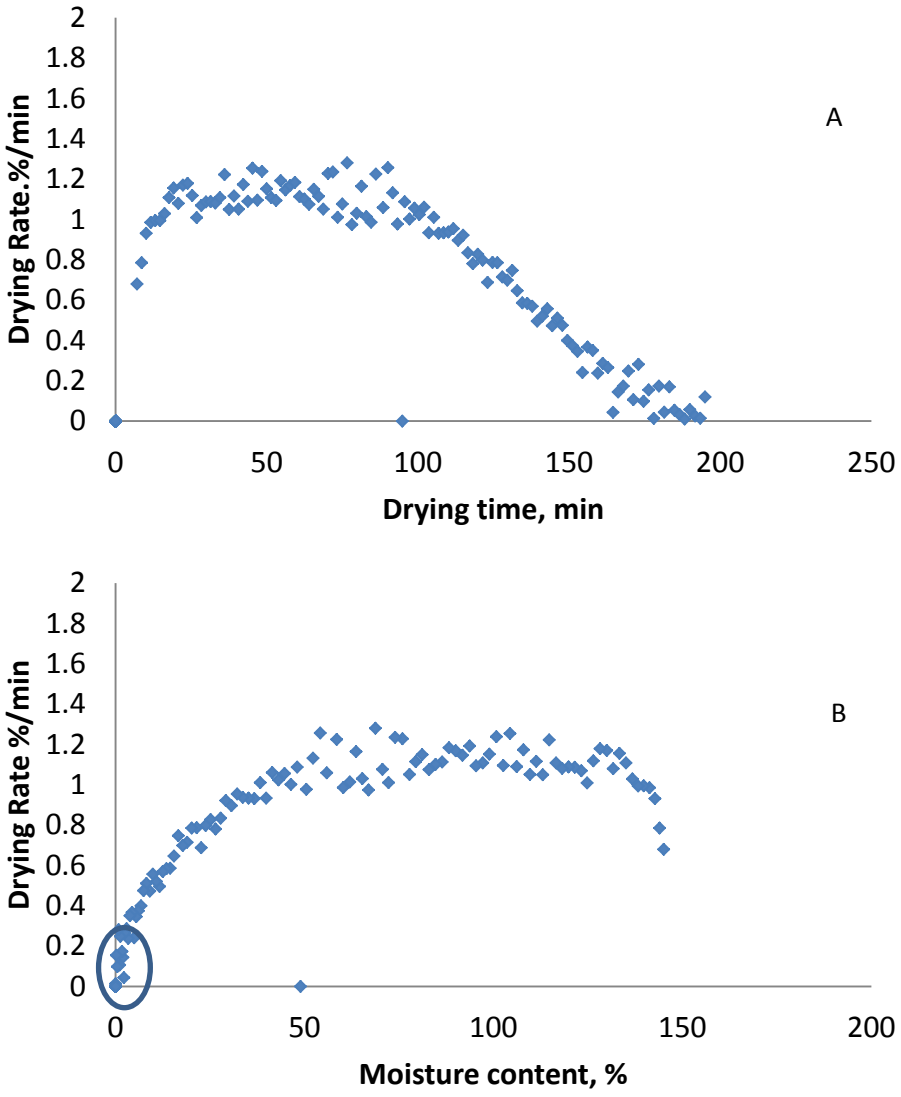

Figure 4.15 Drying rate as a function of time (A) and moisture content (B) for a bed inlet temperature of 100°C and an air velocity of 0.61 m/s.

4.3.3.2 Drying zone

4.3.3.2.1 Drying zone velocity

Drying zone velocity is based on Figure 4.9, rearranged as Figure 4.16, which indicates a linear portion with nonlinear portions at the beginning and end. Assuming that the bed has unlimited depth and is warmed up, a straight line would occur for any section. As indicated in Figure 4.16, the straight line intersects the Y-axis at MC`. The gap between $MC_i$ and MC` is caused by the energy needed to warm the material to wet bulb temperature. The line intersects the X axis at t_{end}, and separates from the actual drying curve at point of "t_{top}". t_{top} is selected at the begin point of the drying curve separate with the straight line.

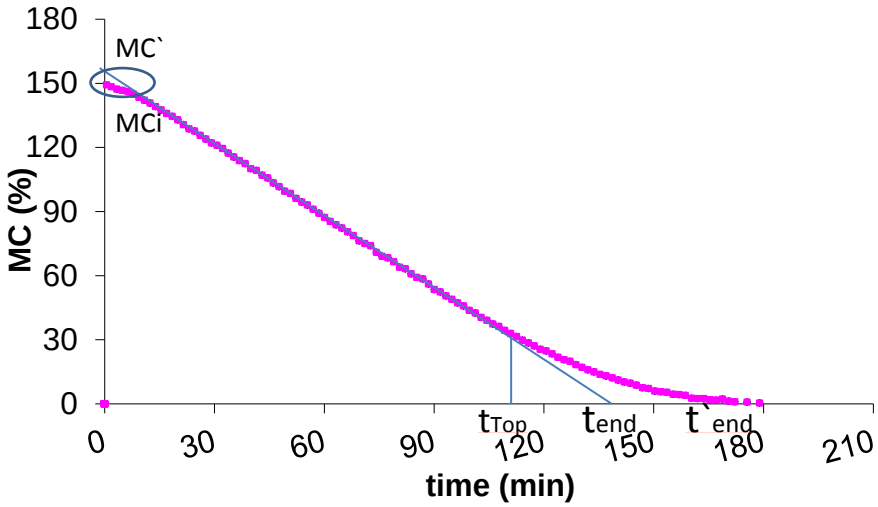

Figure 4.16 Ideal drying curve and measured point.

If one envisions the 23-cm-deep bed as part of an infinitely deep bed, the leading edge of the drying zone would move from the bottom of the bed (at the distributor) to the top of the bed (23 cm above the distributor) from t=0 to $t=t_{top}$ along the straight line in Figure 4.16. Thus, extending the linear portion of the drying curve can be used to estimate the average drying velocity by the formula

$$V_{dz} = \frac{h}{t_{rop}}$$ Equation 4-7

V_{dz}: Velocity of drying zone moving up;

h: height of the bed;

t_{Top}: time of drying zone reaching the top layer.

The drying velocities are shown in Table 4.8 and plotted in Figure 4.17 as a function of temperature. As expected, the drying zone velocity is increased by the increasing of air velocity and temperature, which can be explained by the heat and mass balances (Lerman and Wennberg 2011). The drying velocities also confirmed by the predict model. The formula of the data analysis in multiple linear regression (p-value < 0.05, R^2 =0.97) is:

$$V_{dz} = 10^{-4} \times [-1.210+(0.01447\times T)+(9.424 \times V)+(0.4372\times T\times V)]$$

Equation 4-8

Table 4.8 Data of drying zone speed and drying zone width.

Temp	Vel	h	$t`_{end}$	t_{Top}	V_{dz}	W_{dz}
℃	m/s	m	min	min	m/min	m
93	0.33	0.2286	200	140	1.63E-03	9.78E-02
98	0.33	0.2286	175	122	1.87E-03	9.91E-02
146	0.33	0.2286	114	80	2.86E-03	9.72E-02
78	0.61	0.2286	173	93	2.46E-03	1.97E-01
98	0.61	0.2286	114	74	3.09E-03	1.24E-01
147	0.61	0.2286	86	54	4.23E-03	1.35E-01
196	0.61	0.2286	55	36	6.35E-03	1.21E-01
64	0.81	0.2286	116	74	3.09E-03	1.30E-01
99	0.81	0.2286	78	53	4.31E-03	1.08E-01
147	0.81	0.2286	61	35	6.53E-03	1.70E-01
196	0.81	0.2286	50	28	8.16E-03	1.80E-01
96	0.33	0.2286	230	134	1.71E-03	1.64E-01
100	0.33	0.2286	160	119	1.92E-03	7.87E-02
146	0.33	0.2286	123	87	2.63E-03	9.47E-02
83	0.61	0.2286	126	84	2.72E-03	1.14E-01
98	0.61	0.2286	113	69	3.31E-03	1.46E-01
147	0.61	0.2286	70	46	4.97E-03	1.19E-01
196	0.61	0.2286	66	45	5.08E-03	1.07E-01
65	0.81	0.2286	140	83	2.75E-03	1.57E-01
98	0.81	0.2286	79	50	4.57E-03	1.33E-01
147	0.81	0.2286	63	35	6.53E-03	1.83E-01
99	0.33	0.2286	232	136	1.68E-03	1.61E-01
78	0.61	0.2286	154	96	2.38E-03	1.38E-01
98	0.61	0.2286	100	69	3.31E-03	1.03E-01
147	0.61	0.2286	84	55	4.16E-03	1.21E-01
196	0.81	0.2286	45	31	7.37E-03	1.03E-01
54	0.61	0.2286	244	141	1.62E-03	1.67E-01
98	0.61	0.2286	120	66	3.46E-03	1.87E-01
147	0.61	0.2286	75	48	4.76E-03	1.29E-01
195	0.61	0.2286	57	40	5.72E-03	9.72E-02

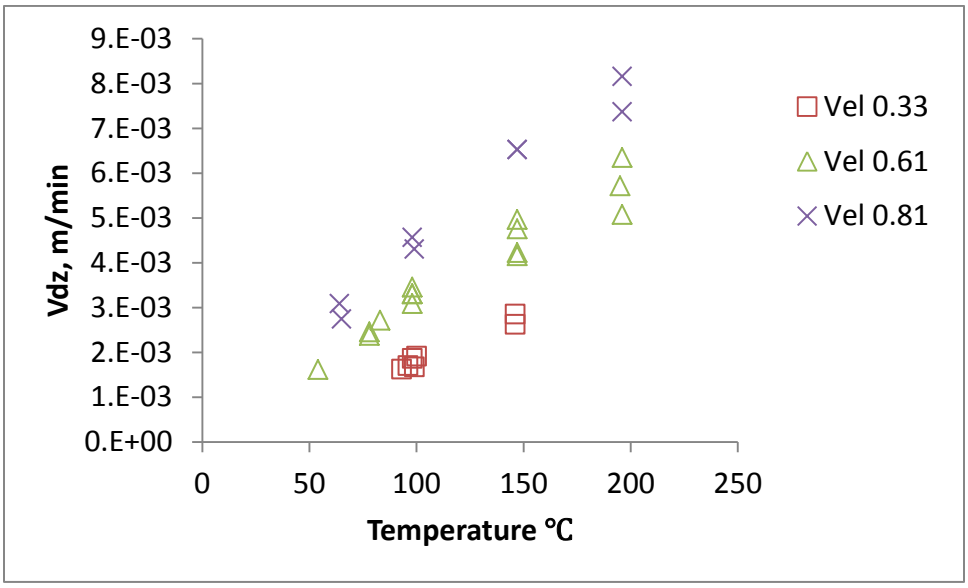

Figure 4.17 Plot of drying zone velocity versus temperature at different air velocities.

4.3.3.2.2 Drying zone width

Drying zone width can be determined from the difference between when the upper bound of the drying zone reaches the top of the bed and when the bed is dry, $t`_{end} - t_{top.}$ Multiplying this value times V_{dz} gives the width of the drying zone (Equation 4-9). The data is shown in Table 4.8 and plotted in Figure 4.18 as a function of temperature and air velocity.

$$W = V_{dz} * (t`_{end} - t_{top}) \qquad \text{Equation 4-9}$$

An ANOVA of the multiple linear regression model with drying zone width as the dependent variable and temperature and air velocity as independent variables showed a significant increase in drying zone width with air velocity (p-value =0.03) and a weak relationship with temperature (p-value= 0.057). Because the moisture

content versus time curve is asymptotic to the abscissa, t'_{end} is difficult to accurately determine from the experimental data. The deep bed model (discussed in section 4.3.4) was run to verify the result and it predicted the drying zone widths shown in Table 4.9 for a final MC of 4% at the lower boundary of drying zone. The model indicates that the drying zone width increases with increasing air which matches the trend for velocity in the experimental data. The trend for temperature based on the model is weaker than that for air velocity which may help to explain the lack of a significant trend in the experimental data. The range of predicted values from the model (Table 4.9, 0.11 to 0.18 m) is in good agreement with the range estimated from the experimental data (Table 4.8, 0.08 to 0.20 m). The average drying zone width from the experimental data (Table 4.8, 0.133 m) is similar to the average from the model (Table 4.9, 0.144 m).

Table 4.9 Drying zone width predict by deep layer model.

Air velocity	Temperature (℃)			
	50	100	150	200
(m/s)	m	m	m	m
0.3	0.13	0.13	0.11	/
0.6	0.16	0.15	0.13	0.13
0.9	0.18	0.17	0.15	0.14

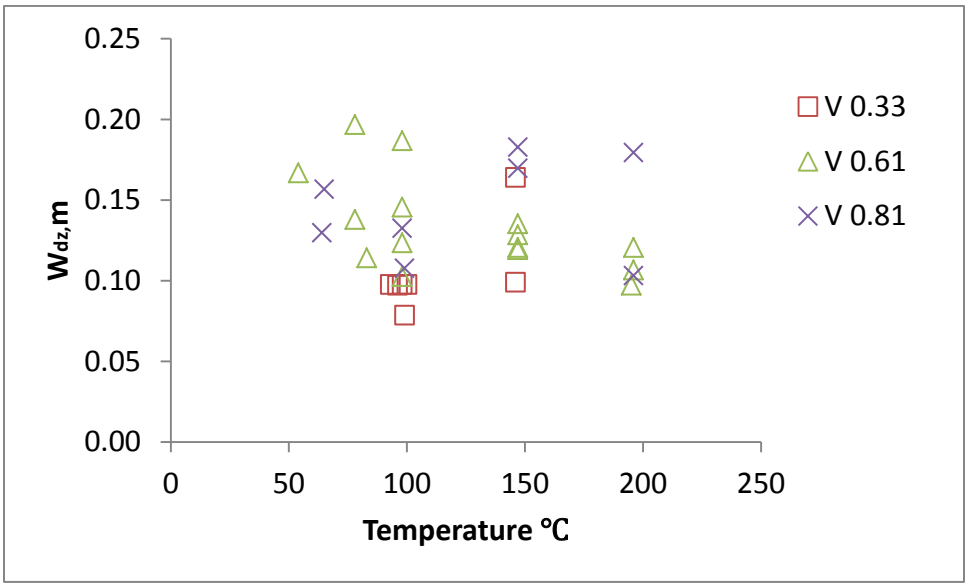

Figure 4.18 Plot of drying zone width versus temperature with groups of velocity.

4.3.4 Modeling bed drying

4.3.4.1 Model introduction

A bed drying model developed at Oregon State University was used in this work. The model divides the bed into layers. The drying air enters the bottom layer and the thin layer drying function is used to obtain a drying rate. The model then calculates the air temperature and humidity leaving the first layer. This air enters the second layer and the calculation is repeated to the top of the bed. A layer is set to approximately 0.5 cm. Mass and energy balances are maintained for each layer. With the model and the thin-layer drying function it is possible to predict drying time or final moisture content given other parameters such as initial moisture content, entering air temperature, and entering air velocity. The moisture content and gas temperature for any bed location can also be predicted.

An example of output from the deep-layer prediction model is shown in Figures 4.19 to 4.22. The parameters were 156% initial moisture content, 7% final moisture content, and a constant 100°C inlet temperature (Figure 4.19) for these figures. The drying time is 163 minutes.

Figure 4.20 gives the average MC versus time and indicates there is a linear portion with a non-linear tail. The drying zone is completely within the bed and saturated air leaves the bed during within the linear portion. The top of the drying zone reaches the top of the bed at the beginning of the nonlinear portion. This graph should is similar to the experimental data in Figure 4.9.

Figure 4.21 shows the MC as a function of bed depth at the end of drying. The bottom of the bed is dry and there is a small zone of material at the top in which the moisture content approaches 50%. This is the drying zone and begins at approximately 0.5 ft.

Figure 4.22 shows the gas temperature versus bed depth and provides similar information as Figure 4.21. It indicates that the lower portion is dry (little or no temperature change occurs) while drying is occurring in the top portion and temperature of the gas is reduced due to evaporation. One benefit of the deep bed drying model is that we can easily analyze the drying zone, which is hard to analyze on the experimental data due to noise data and measurement inaccuracies as discussed in section 4.3.3.2.

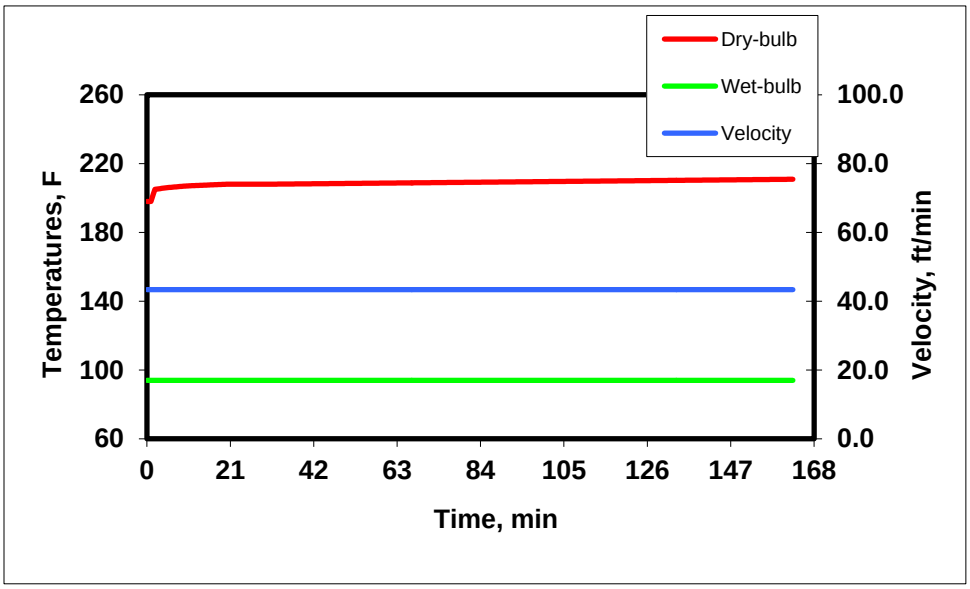

Figure 4.19 Dry bulb temperatures, wet bulb temperature and air velocity.

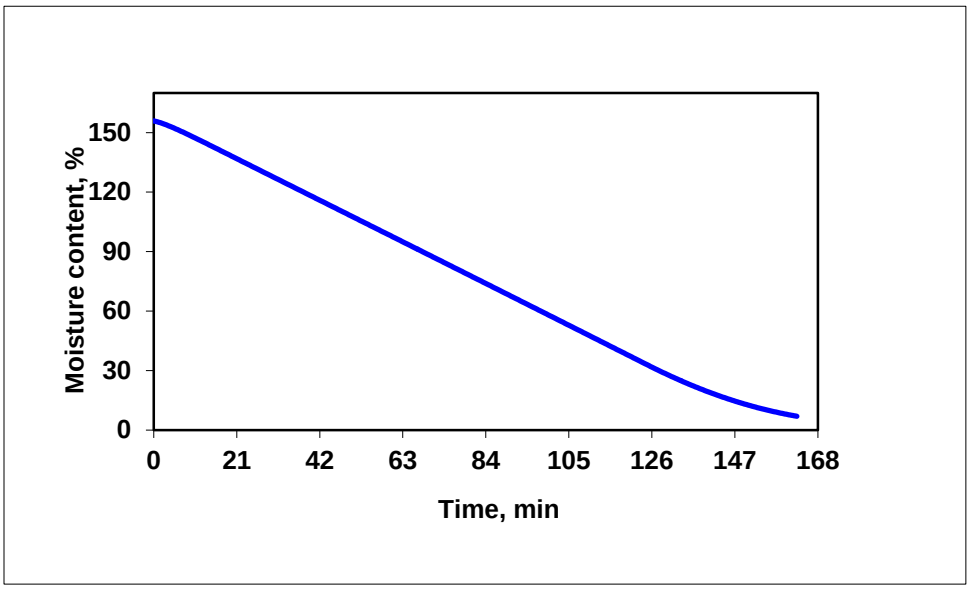

Figure 4.20 Predicted moisture content versus time for deep bed drying.

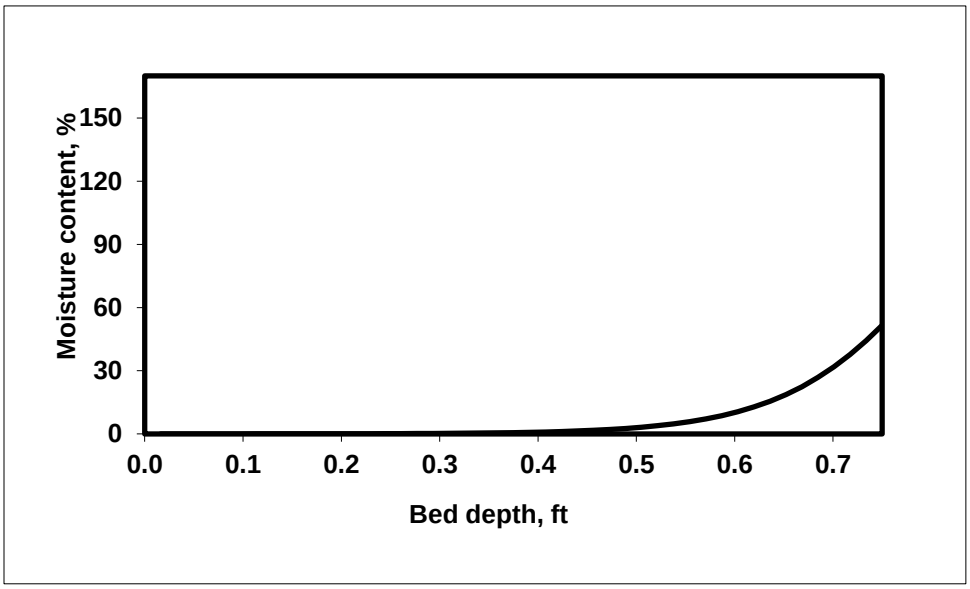

Figure 4.21 Moisture content at each layer at the end of drying.

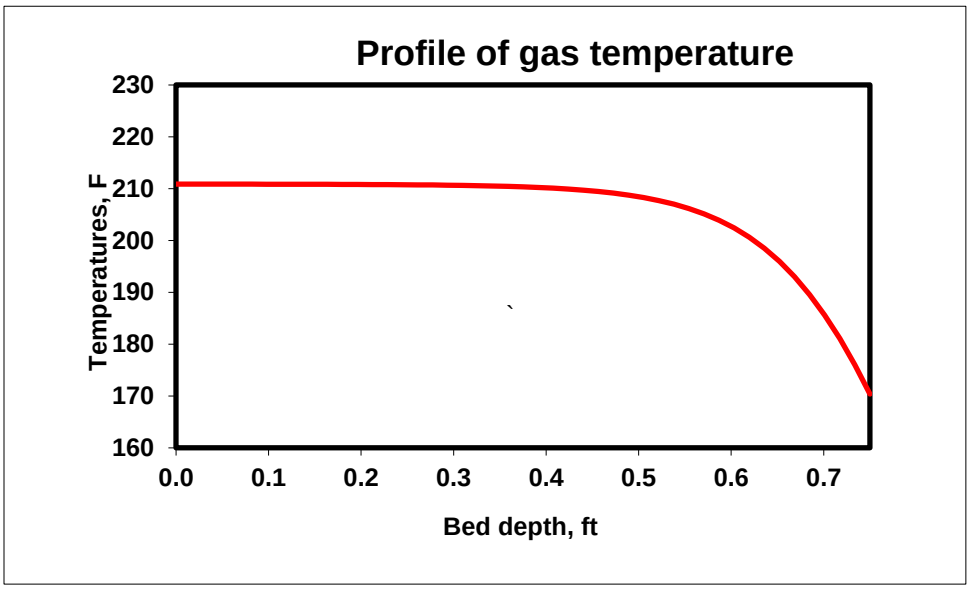

Figure 4.22 Gas temperature at each depth at the end of drying.

4.3.4.2 Comparison of the bed model to experimental data

Tables 4.10 and 4.11 contain predicted drying times from the model and actual drying times from the experiment. The differences between the experimental drying times (third column) and the times predicted by the model were considerable. This difference was attributed to channeling of air through the bed.

A linear regression analysis was done for the data with a 12% final MC. The dependent variable was the time difference between the experiment and the model. The independent variables were temperature and air velocity. The regression did not show a relationship between the difference and temperature or velocity. This further suggested that the 33% channeling of the air through the bed could be compensated for by adding a factor to the model. The right columns in Table 4.10 show the predicted drying times and the percent difference from the experimental time after applying the correction factor. The agreement is much improved. The mean difference between the model and the experimental results after the channeling factor is -2.9%. Table 4.11 shows the similar data on final MC 7% and mean difference is -5.1%.

4.3.4.3 Comparison between model and experiment data

In order to get a better understanding of the model predictions, all the group 1 and group 2 data are compared with the model in Figures 4.23 and 4.24. Each chart in Figure 4.23 is for a single temperature and shows different air velocities

Table 4.10 Predicted and experimental data for a final moisture content of 12%.

	Temperaturee	Velocity	Time, min				
			Final MC to 12%				
	℃	m/s	Experiment	Model	% Dif	Adj-33.3%	% Dif
Group 1	50	0.33	167.5	116.3	-30.6	169.3	1.1
	50	0.61	127	80.7	-36.5	117.3	-7.6
	50	0.81	96	72	-25.0	104.3	8.6
	100	0.33	147.5	111.7	-24.3	165.0	11.9
	100	0.61	93	60.3	-35.2	88.3	-5.1
	100	0.81	65	47.3	-27.2	69.0	6.2
	150	0.33	98.6	72.3	-26.7	106.7	8.2
	150	0.61	71	42.7	-39.9	62.3	-12.3
	150	0.81	45.5	31.7	-30.3	46.0	1.1
	200	0.61	47	30	-36.2	44.0	-6.4
	200	0.81	35	24.3	-30.6	35.3	0.9
Group 2	50	0.33	181	114	-37.0	165.3	-8.7
	50	0.61	110	75.7	-31.2	109.3	-0.6
	50	0.81	117	70	-40.2	101.0	-13.7
	100	0.33	140	103.3	-26.2	152.0	8.6
	100	0.61	90	58.7	-34.8	85.3	-5.2
	100	0.81	65	47	-27.7	68.3	5.1
	150	0.33	102	72.3	-29.1	106.7	4.6
	150	0.61	59	42	-28.8	61.7	4.6
	150	0.81	47	30.3	-35.5	44.0	-6.4
	200	0.61	51	30.3	-40.6	44.3	-13.1
	200	0.81	34	24.3	-28.5	35.3	3.8
Group 3	50	0.33	185	109.7	-40.7	160.0	-13.5
	50	0.61	124	79.3	-36.0	115.3	-7.0
	100	0.61	113	59.7	-47.2	87.3	-22.7
	150	0.61	66	42	-36.4	61.3	-7.1
	200	0.81	36	24.3	-32.5	35.7	-0.8
Group 4	50	0.61	202	127.3	-37.0	188.0	-6.9
	100	0.61	100	61.3	-38.7	89.7	-10.3
	150	0.61	64	43.7	-31.7	63.7	-0.5
	200	0.61	48.5	31	-36.1	45.3	-6.6

Table 4.11 Predicted and experimental data for a final moisture content of 7%.

	Temperature	Velocity	Time,min				
			Final MC to 7%				
	℃	m/s	Elapsed	Model	% Dif	Adj-33.3%	% Dif
Group 1	50	0.33	182.5	125.3	-31.3	231.7	27.0
	50	0.61	148	88.3	-40.3	127.3	-14.0
	50	0.81	104	79.7	-23.4	114.3	9.9
	100	0.33	160.5	120.7	-24.8	177.0	10.3
	100	0.61	101	66	-34.7	95.3	-5.6
	100	0.81	70	52	-25.7	75.0	7.1
	150	0.33	107.6	77.3	-28.2	124.3	15.5
	150	0.61	78	46	-41.0	66.7	-14.5
	150	0.81	51.5	34.7	-32.6	52.3	1.6
	200	0.61	51	32.3	-36.7	47.0	-7.8
	200	0.81	38	26.3	-30.8	38.0	0.0
Group 2	50	0.33	203	122.7	-39.6	176.7	-13.0
	50	0.61	128	82.3	-35.7	118.3	-7.6
	50	0.81	133	77.3	-41.9	110.7	-16.8
	100	0.33	149	111.7	-25.0	163.0	9.4
	100	0.61	99	64	-35.4	92.7	-6.4
	100	0.81	73	51.7	-29.2	74.3	1.8
	150	0.33	110	77.7	-29.4	122.7	11.5
	150	0.61	64	45.7	-28.6	66.0	3.1
	150	0.81	54	33.3	-38.3	47.7	-11.7
	200	0.61	55	32.7	-40.5	47.3	-14.0
	200	0.81	37	26.3	-28.9	38.0	2.7
Group 3	50	0.33	205	118	-42.4	171.0	-16.6
	50	0.61	146	86.7	-40.6	125.0	-14.4
	100	0.61		65.3		94.7	
	150	0.61	70	45.3	-35.3	65.7	-6.1
	200	0.81	39	26.3	-32.6	38.0	-2.6
Group 4	50	0.61	224	138.3	-38.3	202.7	-9.5
	100	0.61	109	67	-38.5	96.7	-11.3
	150	0.61	69	47	-31.9	68.0	-1.4
	200	0.61	51.5	33.3	-35.3	48.3	-6.2

using the group 1 experiment data. Each chart in Figure 4.24 is for a single air velocity and shows drying curves for different temperatures. From these graphs, we can conclude that the model fit the data well, the pseudo R^2 are between 0.839 and 0.996 calculated in Appendix 3. The pseudo R^2 is a goodness of fit measure, and higher values approaching to 1 would indicate better fit. Pseudo R^2 is using here because R^2 has the assumption of linear model. This pseudo R^2 is calculated in the same way as R^2.

4.3.4.4 Model prediction for Douglas-fir

The deep bed drying model can predict the drying for Douglas-fir, using the thin-layer model for hemlock (Figure 4.25). The pseudo R^2 of 100℃ is 0.985 and 0.993 for 150℃. The lack of a difference in the drying characteristics of these two species may be because they have a similar specific gravity and they were the same size.

Group 1:

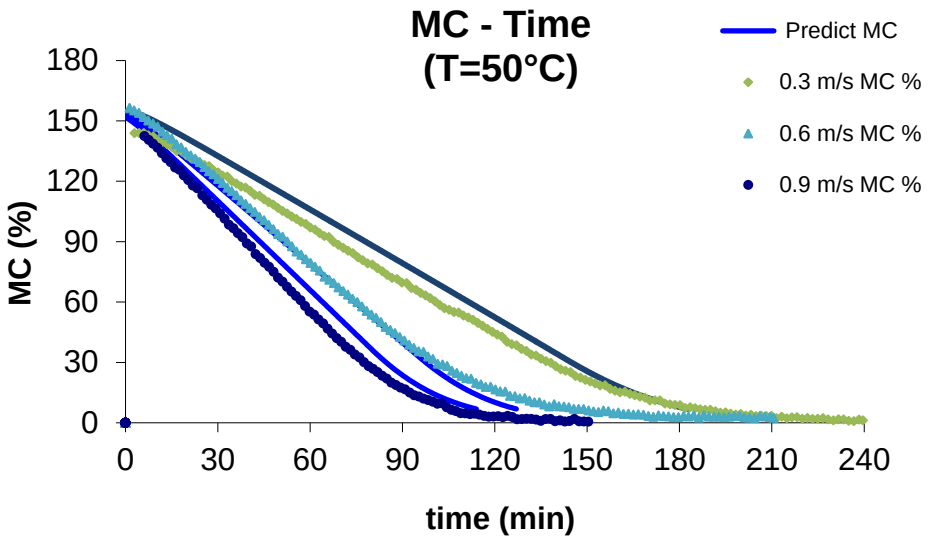

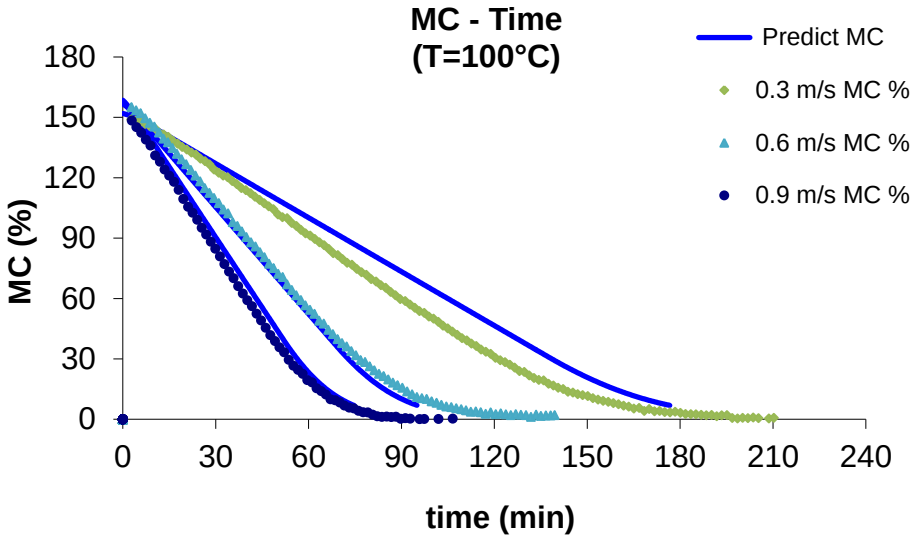

Figure 4.23 Comparison of experiment curve with predicted curve showing the effect of air velocity on drying time.

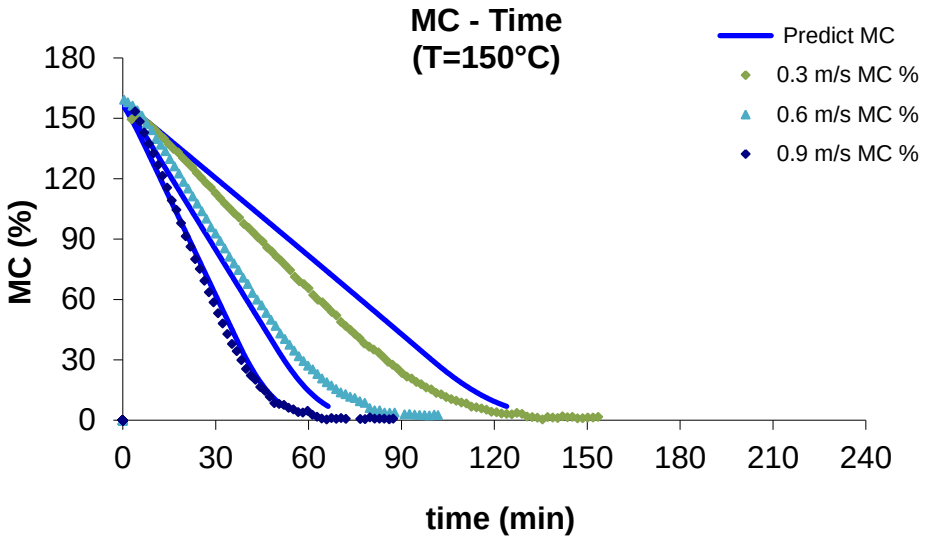

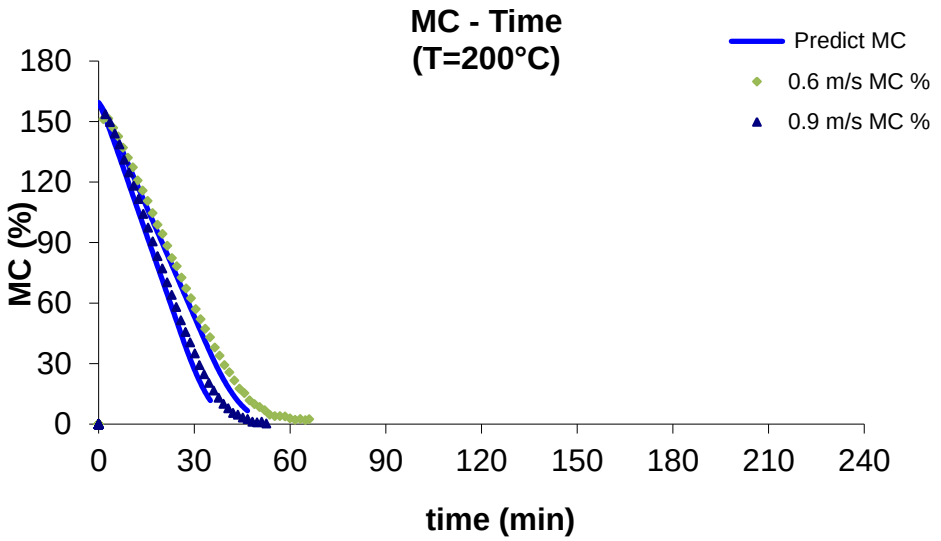

Figure 4.23 Comparison of experiment curve with predicted curve showing the effect of air velocity on drying time (continued).

Group 2:

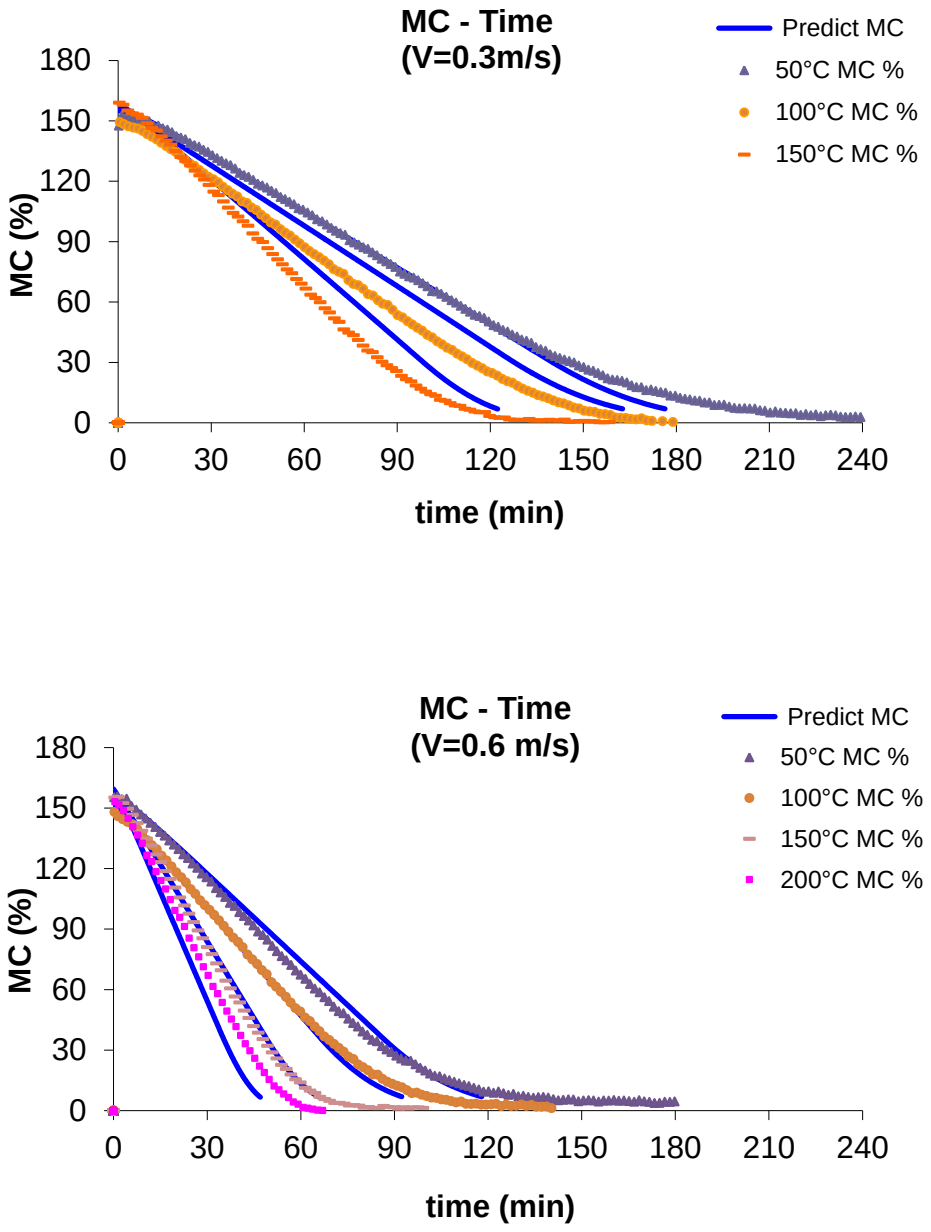

Figure 4.24 Comparison of experiment curves with predicted curves showing the effect of temperature on drying time.

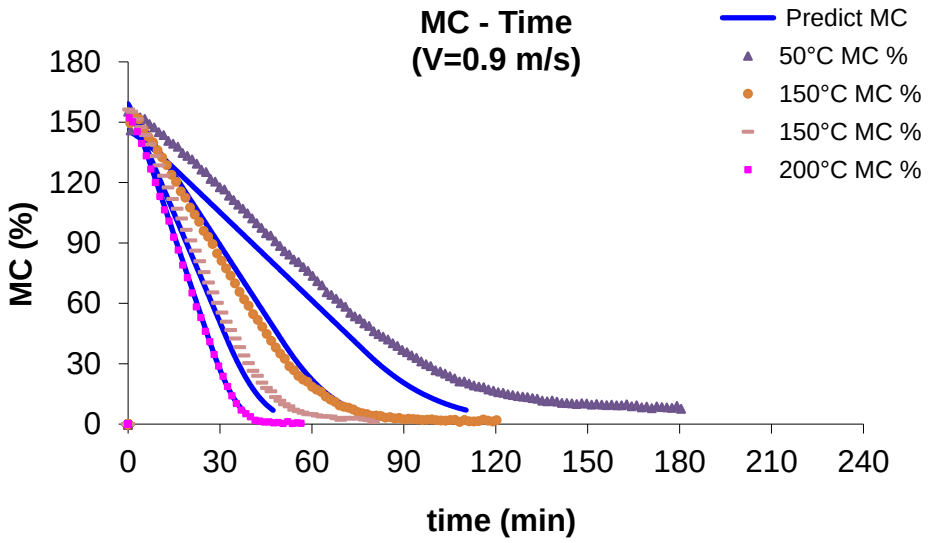

Figure 4.24 Comparison of experiment curves with predicted curves showing the effect of temperature on drying time (continued).

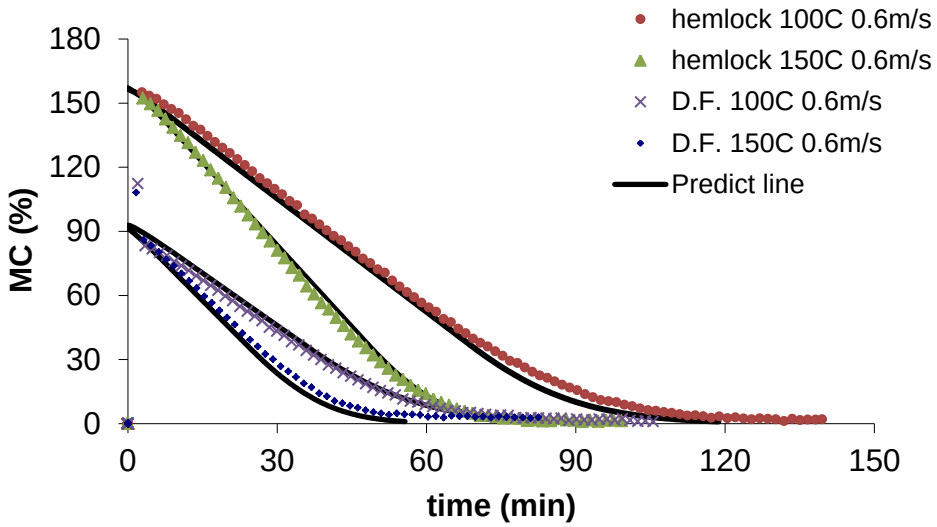

Figure 4.25 Comparison of experiment curve with predict curve on effect of species on drying time.

4.3.4.5 Model applications

With a deep bed drying model, the drying time in a fixed bed can be predicted given the initial moisture content and the inlet temperature, gas velocity, and humidity. Alternatively, the temperature and gas velocity required to dry in a given time could be determined. This is significant for determining the size of a dryer needed to process a certain amount of biomass. With little extra calculation, the designer could also determine the energy requirements for a dryer and size the burner.

The model also predicts the vertical moisture content within the dryer and may help designers determine the appropriate bed depth. The moisture variability leaving a dryer can also be calculated which may impact how downstream operations are performed. The vertical moisture profile is also important for determining the depth of the biomass bed. A designer would want the bed to be deep enough to contain the drying zone for most of the biomass residence time to maintain dryer efficiency.

The model does not help the designer determine when channeling will occur. It also does not indicate when particle entrainment and carry over would occur.

CHAPTER 5. Conclusions

Thin-layer drying and deep bed drying of wood particles at various drying temperature and air velocity were conducted to develop a prediction model for the drying behavior of particles and the drying behavior of a bed.

A simple one-parameter Newton model can describe the thin-layer drying in a fixed bed. The parameter was affected by temperature and air velocity. The Newton model developed for hemlock particles also worked well for Douglas-fir particles.

A drying zone was observed based on bed temperatures taken at different heights. It was also predicted by the deep bed model. The drying zone in this work was approximately 13 cm. An industrial dryer needs to be designed with a bed deep enough to fully contain the drying zone to maximize the efficiency of the dryer. The drying zone moves upward as drying proceeds with the velocity of the drying zone affected by drying temperature and air velocity.

The material in an industrial dryer would need to be mixed or a dryer would need to be designed with stages to avoid having very dry material at the bottom of the bed and very wet material at the top of the bed at the end of drying. Channeling of air through the fixed bed may pose a problem for dryer efficiency in deep bed drying.

The drying curves determined by the experimental method using a thin layer can be used to predict the drying behavior in a deep bed.

Bibliography

Bartuska, A. (2006). "Why biomass is important: The role of the USDA forest service in managing and using biomass for energy and other uses." USDA Forest Service, Washington, DC. http://www.fs.fed.us/research/pdf/biomass_importance.pdf

Bengtsson, P. (2008). "Experimental analysis of low-temperature bed drying of wooden biomass particles." Drying Technology **26**(5): 602-610.

Corder, S. E. (1958). "Suspension drying of sawdust." Forest Products Journal **8**(1): 5.

Ertekin, C. and O. Yaldiz (2004). "Drying of eggplant and selection of a suitable thin layer drying model." Journal of Food Engineering **63**(3): 349-359.

EUBIA (2007). " Biomass characteristics " European Biomass Industry Association. Accessed on 29 June 2012 at 13:20. http://www.eubia.org/115.0.html

FAO (1982). "Appropriate technology in forestry." Forestry Paper **No. 31**.

Forest Products Laboratory (2010). "Wood handbook—Wood as an engineering material.": General Technical Report FPL-GTR-190. Madison, WI: U.S. Department of Agriculture, Forest Service, Forest Products Laboratory. 508 p.

Hakkila, P. (1989). "Utilization of residual forest biomass." Springer Series in Wood Science Springer-Verlag New York Inc. 568.

Hewett, C. E. (1981). "Wood energy in the united states." Annual Review of Energy **6**(1): 139.

Lerman, P. and O. Wennberg (2011). "Experimental method for designing a biomass bed dryer." Biomass and Bioenergy **35**: S31-S39.

Maloney, T. M. (1993). "Modern particleboard & dry-process fiberboard manufacturing (Updat ed.)." San Francisco: Miller Freeman.

Midilli, A. K., H.; Yapar,Z. (2002). "A new model for single-layer drying." Drying Technology **20**(7): 1503–1513.

Milota, M. R., C. D. West and I. D. Hartley (2005). "Gate-to-gate life-cycle inventory of softwood lumber production." Wood and Fiber Science **37**(Corrim Special Issue): 47 – 57.

Milota, M. R. and J. B. Wilson (1989). "Analysis of the Fluidized-Bed Drying of Wood Particles." Wood and Fiber Science **22**(2): 193-203.

Moreno, R. A. n., G. ; Reyes, A. ; Alvarez, P. ; (2004). "Drying Characteristics of Forest Biomass Particles of Pinus radiata." Biosystems Engineering **88**(1): 105-115.

Mujumdar, A. S. (1987). "Handbook of industrial drying." Springer Verlag, cop. Berlin.

Pardeshi, I. L., S. Arora and P. A. Borker (2009). "Thin-Layer Drying of Green Peas and Selection of a Suitable Thin-Layer Drying Model." Drying Technology **27**(2): 288-295.

Parikka, M. (2004). "Global biomass fuel resources." Biomass & Bioenergy **27**(6): 613-620.

Perlack, R. D., L. L. Wright, A. F. Turhollow, R. L. Graham, B. J. Stokes and D. C. Erbach (2005). "Biomass as Feedstock for A Bioenergy and Bioproducts Industry: The Technical Feasibility of a Billion-Ton Annual Supply." Accessed on 29 June 2012. http://www.dtic.mil/cgi-bin/GetTRDoc?AD=ADA436753

Roos, C. (2008). "Biomass Drying and Dewatering for Clean Heat and Power." Olympia,WA: Northwest CHP Application Center.

Sissine, F. (2007). "Energy Independence and Security Act of 2007: A Summary of Major Provisions." CRS Report for Congress, order code RL34294.

Stupak, I., A. Asikainen, M. Jonsell, E. Karltun, A. Lunnan, D. Mizaraite, K. Pasanen, H. Parn, K. Raulundrasmussen and D. Roser (2007). "Sustainable utilisation of forest biomass for energy—Possibilities and problems: Policy, legislation, certification, and recommendations and guidelines in the Nordic, Baltic, and other European countries." Biomass and Bioenergy **31**(10): 666-684.

Wikipedia (2012). "Coefficient of determination." Wikipedia, last modified on 13 June 2012 at 19:20. http://en.wikipedia.org/wiki/Coefficient_of_determination.

Yrjola, J. S., Jaakko J. (2002). "Modelling and practical operation results of a dryer for wood chips." Drying Technology **20**(6): 1077–1099.

Zerbe, J. I. (2006). "Thermal energy, electricity, and transportation fuels from wood." Forest Products Journal **56**(1): 6-14.

Appendices

Appendix 1: Statistical analysis for the models

Statistical analysis for the models				
Drying conditions		Model Name	RMSE	adj-R^2
Air flow m/s	Temperature °C			
0.3	50	Newton	0.0461	0.9836
0.3	50	Henderson and Pabis	0.3958	-0.2083
0.3	50	Logritmic	0.3169	0.2251
0.3	50	Two term	0.4172	-0.3426
0.3	50	Two term exponential	0.3958	-0.2083
0.3	50	Diffusion approximation	0.2767	0.4096
0.3	50	Verma et al.	0.0329	0.9917
0.3	50	Modified Henderson and Pabis	0.0373	0.9893
0.3	50	Wang and Singh	0.0725	0.9595
0.3	50	Thompson	7.7620	0.9642
0.3	100	Newton	0.0490	0.9811
0.3	100	Henderson and Pabis	0.3653	-0.0484
0.3	100	Logritmic	0.0518	0.9789
0.3	100	Two term	0.3850	-0.1648
0.3	100	Two term exponential	0.3653	-0.0484
0.3	100	Diffusion approximation	0.3056	0.2663
0.3	100	Verma et al.	0.0461	0.9833
0.3	100	Modified Henderson and Pabis	0.0522	0.9786
0.3	100	Wang and Singh	0.0904	0.9358
0.3	100	Thompson	4.1630	0.9588

0.3	150	Newton	0.0622	0.9727
0.3	150	Henderson and Pabis	0.4837	-0.6467
0.3	150	Logritmic	0.3574	0.1007
0.3	150	Two term	0.5098	-0.8297
0.3	150	Two term exponential	0.4837	-0.6467
0.3	150	Diffusion approximation	0.2334	0.6166
0.3	150	Verma et al.	0.0461	0.9851
0.3	150	Modified Henderson and Pabis	0.0522	0.9808
0.3	150	Wang and Singh	0.0493	0.9829
0.3	150	Thompson	1.8920	0.9513
0.3	200	Newton	0.0507	0.9822
0.3	200	Henderson and Pabis	0.4165	-0.1990
0.3	200	Logritmic	0.3448	0.1782
0.3	200	Two term	0.4390	-0.3322
0.3	200	Two term exponential	0.4165	-0.1990
0.3	200	Diffusion approximation	0.3711	0.0483
0.3	200	Verma et al.	0.0259	0.9954
0.3	200	Modified Henderson and Pabis	0.0294	0.9940
0.3	200	Wang and Singh	0.0577	0.9770
0.3	200	Thompson	1.7270	0.9594
0.6	50	Newton	0.0358	0.9876
0.6	50	Henderson and Pabis	0.3301	-0.0525
0.6	50	Logritmic	0.0220	0.9953
0.6	50	Two term	0.3480	-0.1694
0.6	50	Two term exponential	0.3301	-0.0525
0.6	50	Diffusion approximation	0.3118	0.0609
0.6	50	Verma et al.	0.0327	0.9897
0.6	50	Modified Henderson and Pabis	0.0371	0.9867
0.6	50	Wang and Singh	0.0867	0.9273
0.6	50	Thompson	6.5850	0.9544

0.6	100	Newton	0.0370	0.9886
0.6	100	Henderson and Pabis	0.3201	0.1474
0.6	100	Logritmic	0.2722	0.3835
0.6	100	Two term	0.3395	0.0408
0.6	100	Two term exponential	0.3201	0.1474
0.6	100	Diffusion approximation	0.4550	-0.7227
0.6	100	Verma et al.	0.0328	0.9911
0.6	100	Modified Henderson and Pabis	0.0378	0.9881
0.6	100	Wang and Singh	0.1126	0.8945
0.6	100	Thompson	4.5750	0.9137
0.6	150	Newton	0.0394	0.9865
0.6	150	Henderson and Pabis	0.3413	-0.0102
0.6	150	Logritmic	0.2819	0.3107
0.6	150	Two term	0.3579	-0.1112
0.6	150	Two term exponential	0.3413	-0.0102
0.6	150	Diffusion approximation	0.2676	0.3789
0.6	150	Verma et al.	0.0418	0.9848
0.6	150	Modified Henderson and Pabis	0.0468	0.9810
0.6	150	Wang and Singh	0.0800	0.9446
0.6	150	Thompson	2.1620	0.9126
0.6	200	Newton	0.0421	0.9868
0.6	200	Henderson and Pabis	0.3693	-0.0156
0.6	200	Logritmic	0.3160	0.2563
0.6	200	Two term	0.3893	-0.1284
0.6	200	Two term exponential	0.3693	-0.0156
0.6	200	Diffusion approximation	0.2305	0.6043
0.6	200	Verma et al.	0.0197	0.9971
0.6	200	Modified Henderson and Pabis	0.0224	0.9963
0.6	200	Wang and Singh	0.0762	0.9567
0.6	200	Thompson	0.9742	0.9797

0.9	50	Newton	0.0690	0.9468
0.9	50	Henderson and Pabis	0.3370	-0.2676
0.9	50	Logritmic	0.0494	0.9727
0.9	50	Two term	0.3552	-0.4085
0.9	50	Two term exponential	0.3370	-0.2676
0.9	50	Diffusion approximation	0.2936	0.0375
0.9	50	Verma et al.	0.0464	0.9760
0.9	50	Modified Henderson and Pabis	0.0526	0.9691
0.9	50	Wang and Singh	0.0891	0.9114
0.9	50	Thompson	4.6280	0.9714
0.9	100	Newton	0.0217	0.9958
0.9	100	Henderson and Pabis	0.3111	0.1313
0.9	100	Logritmic	0.2603	0.3919
0.9	100	Two term	0.3279	0.0348
0.9	100	Two term exponential	0.3111	0.1313
0.9	100	Diffusion approximation	0.3398	-0.0365
0.9	100	Verma et al.	0.0234	0.9951
0.9	100	Modified Henderson and Pabis	0.0266	0.9937
0.9	100	Wang and Singh	0.1009	0.9085
0.9	100	Thompson	3.1900	0.9456
0.9	150	Newton	0.0326	0.9911
0.9	150	Henderson and Pabis	0.3621	-0.1004
0.9	150	Logritmic	0.2904	0.2923
0.9	150	Two term	0.3817	-0.2227
0.9	150	Two term exponential	0.3621	-0.1004
0.9	150	Diffusion approximation	0.2566	0.4474
0.9	150	Verma et al.	0.0359	0.9892
0.9	150	Modified Henderson and Pabis	0.0407	0.9861
0.9	150	Wang and Singh	0.0673	0.9620
0.9	150	Thompson	1.8110	0.9299

0.9	200	Newton	0.0602	0.9698
0.9	200	Henderson and Pabis	0.3169	0.1626
0.9	200	Logritmic	0.2764	0.3631
0.9	200	Two term	0.3341	0.0696
0.9	200	Two term exponential	0.3169	0.1626
0.9	200	Diffusion approximation	0.4340	-0.5701
0.9	200	Verma et al.	0.0335	0.9906
0.9	200	Modified Henderson and Pabis	0.0380	0.9879
0.9	200	Wang and Singh	0.0599	0.9701
0.9	200	Thompson	1.5220	0.9208
Average		Newton	0.0602	0.9698
		Henderson and Pabis	0.3169	0.1626
		Logritmic	0.2764	0.3631
		Two term	0.3341	0.0696
		Two term exponential	0.3169	0.1626
		Diffusion approximation	0.4340	-0.5701
		Verma et al.	0.0335	0.9906
		Modified Henderson and Pabis	0.0380	0.9879
		Wang and Singh	0.0599	0.9701
		Thompson	1.5220	0.9208

Appendix 2: SAS code used for models one to eight.

```
*Newton model*
proc model data=yh;
parms k;
MR=exp(-k*time);
fit MR/out=m1 outpredict outresid;
run;

*Henderson and Pabis model*
proc model data=yh;
parms a k;
MR=a*exp(-k*time);
fit MR/out=m2 outpredict outresid;
run;

*Lograitmic model*
proc model data=yh;
parms a k c;
MR=a*exp(-k*time)+c;
fit MR/out=m3 outpredict outresid;
run;

*Two term model*
proc model data=yh;
parms a k c g;
MR=a*exp(-k*time)+c*exp(-g*time);
fit MR/out=m4 outpredict outresid;
run;

*Two term exponential model*
proc model data=yh;
parms a k;
MR=a*exp(-k*time)+(1-a)*exp(-k*a*time);
fit MR/out=m5 outpredict outresid;
run;

*Diffusion approximation model*
proc model data=yh;
parms a k b;
MR=a*exp(-k*time)+(1-a)*exp(-k*b*time);
fit MR/out=m6 outpredict outresid;
run;

*Verma et al. model*
proc model data=yh;
parms a k g;
MR=a*exp(-k*time)+(1-a)*exp(-g*time);
```

```
fit MR/out=m7 outpredict outresid;

run;


*Modified Henderson and Pabis model*

proc model data=yh;

parms a k b g c h;

MR=a*exp(-k*time)+b*exp(-g*time)+c*exp(-h*time);

fit MR/out=m8 outpredict outresid;

run;


ods graphics on;

proc mcmc data=yh outpost=predict seed=1234 nmc=100;

ods select Parameters REParameters PostSUmmaries TADpanel ess mcse;

parms a k;

prior a ~ normal(0,sd=100);

prior k ~ normal(0,sd=1000);

mu=a*exp(-k*time);

model MR~normal(mu,var=10);

run;

quit;

ods graphics off;


ods graphics on;

proc mcmc data=yh outpost=predict seed=1234 nmc=100;

ods select Parameters REParameters PostSUmmaries TADpanel ess mcse;

parms a k n b;

prior a ~ normal(0,sd=100);

prior k ~ normal(0,sd=1000);

prior n ~ normal(0,sd=100);

prior b ~ normal(0,sd=1000);

mu=a*exp(-k*time**n)+b*time;

model MR~normal(mu,var=100);

run;

quit;

ods graphics off;
```

Appendix 3: R code used for two models and pseudo R^2

```
library(Sleuth2)

my.try<-read.csv('…/1_2_150.csv')

attach(my.try)

names(my.try)

my.try$log.time<-log(time)

my.try$log.MR<-log(MR)

attach(my.try)

plot(MR~time)


x<-seq(0,50,1)

y<-exp(-0.19208042*x)


lines(x,y)


MR<-exp(-0.212824*time)

time<-seq(0,50,20)

line(time~MR)




# MR=a*exp(-kt)

try.lm1<-lm(log.MR~time)

plot(time,MR)

names(try.lm1)

dum1    <- seq(0,60,length=100)

mod1MR<-
exp(try.lm1$coef[1]+try.lm1$coef[2]*dum1)

lines(mod1MR)



plot(try.lm1)

summary(try.lm1)

anova(try.lm1)


# Model 2: wang and Singh:

# MR=1+at+bt^2

timesquare<-time^2

try.lm3<-lm(MR~1+time+timesquare)

plot(try.lm3)

summary(try.lm3)

anova(try.lm3)


# Model: Thompson,

# t=a*ln(MR)+b*[ln(MR)]^2

log2.MR<-log.MR^2

try.lm4<-lm(time~log.MR+log2.MR)

plot(try.lm4)

summary(try.lm4)

anova(try.lm4)

detach()
```

```
# Pseudo-R^2

MC<-read.csv('D:/HL 1-3-50.csv',header=TRUE)

attach(MC)

plot(MC_pre~time)

plot(MC_exp~time)

SScurv<-sum((MC_exp-MC_pre)^2)


SScurv

SShoriz<-sum((MC_exp-mean(MC_exp))^2)

SShoriz

R2<-1-(SScurv/SShoriz)

R2
```

Appendix 4: Example form for manually-recorded data

Propose:	T= 100C V~15%~0.3m/s Depth = 9 inches							
Experiment Time:	4.27 3:30pm							
Set the save file address:	4.27 4 pm V 0.3 T 100C Depth=9inch.lvm							
Set speed:	15	%	0.3	m/s				
Set temperature:	212	F	100	C				
Depth of the chips:	9	inches	of	mixed wood chips				
Check out whether load cells work right:			YES					
Basket weight:	A	12.67	lbs	C	12.4	lbs		
Basket with wet chips:		A	40.24	lbs		C	39.4	lbs
Whether preheat before Drying process:			YES					
Predict MC:	158	%						
Preheat time:	18	mins						
Texit (F)	190	Tover (F)	179	Tout1,2 (F)	62	Tu (F)	206	208
Set Tare weight:	12.4	lbs						

Drying process:	Time	Weight (lb)			
Start:	20.0	26.4			
Turning point:	190.0		T'exit (F)	192	
End:	220.0	10.6			

	Cool down:						EMC:	0	
Dry chip + basket:		A	23.43	lbs		weight equation parameter		8.2	(0<X<8.2)
Dry chip:	A	10.76	lbs	C	10.60	lbs			
MC:	A	156	%	C	155	%			
Drying time:		170.0	mins						

Appendix 5: Data automatically recorded by LabView.

Load cell						
Time	cell 1	cell 2	cell 3	cell 4	Total Weight	excitation
s	lb	lb	lb	lb	lb	v
Pressure				Air velocity	Temperature	Temperature
Over	bed	under	ΔP		Burner outlet	Setting
in	in	in	in	%	F	F
Teperature sensor						
T exit	T over	T out 1	T out 2	T bed	T under 1	T under 2
F	F	F	F	F	F	F

Notice: On our equipment, the maximum air velocity transform 100%, so 15%= 0.3m/s (need adjust equipment), 23%=0.6m/s, 30%=0.85m/s. Pressure unit was transform to Pa during the data analysis process.